

Drift Chamber Calibration Using Laser Ionization



THE UNIVERSITY
of MANCHESTER

Robert K. Griffiths

A thesis submitted to the University of Manchester for the degree of
Master of Science in the Faculty of Science and Engineering,
Department of Physics and Astronomy.

September 13, 1994

Contents

List of Figures	4
List of Tables	6
Abstract	7
Declaration	8
Copyright	9
1 Introduction	11
1.1 The Drift Chamber	11
1.2 The Forward Muon Spectrometer	12
2 The Drift Cell	16
2.1 Principles And Theory Of Operation	16
2.1.1 Design Detail	18
2.2 The Gas	20
3 The Laser	22
3.1 Description	22
3.2 The Pockels Effect	23
3.3 The Pockels Cell	24
3.4 The Q-Switched Nd:YAG Laser	25
3.5 Beam Theory	29
3.5.1 Modes	29
3.5.2 Waist	30
3.5.3 Focal Length Corrections	31
4 Experimental Results	32
4.1 Experimental Set-Up At Manchester	32
4.2 Initial Studies	33
4.3 Alignment	39

4.3.1	Finding The Middle Of The Cell	39
4.3.2	Where To Take The Data	41
4.4	Investigation Of The Laser's Properties	42
4.4.1	Laser Intensity	42
4.4.2	Beam-Shape Investigation	43
4.5	Time Binning Investigation	46
5	Analysis	49
5.1	Introduction	49
5.2	Ntuples	50
5.3	Box Plots	58
5.4	Profile Histograms	60
5.5	Fitting in PAW	60
5.6	Results	64
6	Discussion	72
7	Conclusion	75
	Bibliography	77

List of Figures

1.1	A Schematic Of The H1 Detector	14
1.2	A Cutaway Of The Entire H1 Detector	15
2.1	A Schematic Of A Drift-Cell	18
2.2	The Electrode Pattern	19
2.3	Simulation Of Drift-Velocity As It Varies With $\frac{E}{p}$	21
3.1	Diagram To Illustrate Stimulated Emission	23
3.2	A Longitudinal Pockels Cell	26
3.3	Energy Level Diagram For Nd:YAG Laser	27
3.4	Illustration Of The Process Of Firing The Laser	28
3.5	Some Beam-Mode Diagrams	29
3.6	A Model Of The Beam Profile As It Nears It's Waist	30
4.1	Schematic Of The Apparatus	33
4.2	Drift-Time Distribution For An Externally-Generated Pulse	34
4.3	Drift-Time Distribution Using Scanner Pulses With Threshold Of 16 Decimal	35
4.4	Simulated Drift-Time Distribution With A New J_0 Card	36
4.5	Drift-time Distribution For Wholly Scanner-Generated Pulses	37
4.6	Direct-Input Externally Generated Pulses	38
4.7	Using The PMT Pulse As Start And Stop	38
4.8	Illustration Of The Measuring Method And How It's Related To The Actual Distance	40
4.9	Variation Of Drift Time With "Scale" Through The Depth Of The Cell	41
4.10	Heights Of Pulses At 730 Volts	44
4.11	Heights Of Pulses At 750 Volts	44
4.12	Parabolic Nature Of The Laser Pulse Heights Against Voltage graph .	45
4.13	The Reticon Array Set-Up	46
4.14	Illustration Of The Time-Binning Investigation	47
5.1	The Drift-Time Distribution When No Cuts Are Applied	54
5.2	The Drift-Time Distribution At The Focal Point	54

5.3	Specifying The Correct Channel From The Flash ADC	55
5.4	Adding A Cut To Stop Cosmic Triggers	55
5.5	Drift-Time Distribution For The First Hit On The Wire.	56
5.6	Cutting Down Pulses Which Are Too High	56
5.7	Eliminating Small Pulses	57
5.8	Eliminating Slightly Larger Pulses	57
5.9	Drift-Time Distribution For Run 2916	59
5.10	Drift-Time Distribution For Run 2916 With A Gaussian Envelope . .	59
5.11	Scatter Plot Of Drift-Time With Focal Distance	61
5.12	Box Plot Derived From The Previous Scatter	61
5.13	Profile Histogram - Central Portion Fitted With Straight Line	62
5.14	Residual Plot Of The Previous Graph	63
5.15	Typical Shape Of The Drift-Time Against Drift-Distance Curve . . .	65
5.16	Profile Histogram Of The Drift-Time Against Drift-Distance Curve .	65
5.17	Variation Of Drift-Velocity With $\frac{E}{p}$ For The Manchester Gas	67
5.18	Variation Of Drift-Velocity With $\frac{E}{p}$ For The H1 Gas	67
5.19	Both The Previous Graphs For Easier Comparison	68
5.20	Real Drift Velocity Against $\frac{E}{p}$ For The Gas At Manchester	68
5.21	Zooming In On The Peak	69
5.22	Scatter in the Drift-times at the same Operating Voltages but differ- ent pressures	70
5.23	Comparison Of Simulation And Real Data	71

List of Tables

5.1	A Table Of PAW Parameters	51
5.2	Collected Data From Drift Velocity Measurements At Various Values Of $\frac{E}{p}$	66

Abstract

A Q-switched Nd:YAG laser was used to ionize Forward Muon Spectrometer gas in a drift chamber built to replicate those used at the Forward Muon Spectrometer at H1. Measurements were taken of the interval between the registration of a pulse when the laser beam is detected by a photomultiplier tube, and the observation of a pulse from the sense wire which can be correlated with the drift distance giving a drift velocity. A value of 4.491 ± 0.035 cm/ μ s is obtained for the drift-velocity of the electrons in the central drift region, and this is compared to the current value of the drift velocity used by H1.

Declaration

No portion of the work referred to in this thesis has been submitted in support of an application for another degree or qualification of this or any other institute of learning.

Copyright

Copyright in text of this thesis rests with the Author. Copies (by any process) either in full, or of extracts, may be made **only** in accordance with the instructions given by the Author and lodged in the John Rylands University Library of Manchester. Details may be obtained from the Librarian. This page must form part of any such copies made. Further copies (by any process) of copies made in accordance with such instructions may not be made without the permission (in writing) of the Author.

The ownership of any intellectual property rights which may be described in this thesis is vested in the University of Manchester, subject to any prior agreement to the contrary, and may not be made available for the use of third parties without the written permission of the University, which will prescribe the terms and conditions of any such agreement.

I Mamgu

Chapter 1

Introduction

The purpose of this investigation is to measure, using laser ionization, the drift velocity of electrons in a drift chamber identical to those used in the Forward Muon Spectrometer in H1, DESY.

1.1 The Drift Chamber

The drift chamber used in this laboratory experiment is a replica of the ones used at the H1 experiment at HERA, DESY¹. There are a few minor differences, such as the materials used in its construction, but the characteristics which dictate the physics (see chapter 2) are the same. The chamber used for this simulation is 12 cm high, 2 cm deep, and about 25 cm long. This is the same height and depth as the actual chambers, but the length is considerably shorter than the real chambers, which have lengths between 40 cm and 240 cm. A drift, or sense wire lies in the middle of the chamber, at a depth of 1 cm, giving a maximum drift distance of 6 cm either side of the central wire.

The drift chamber used here has silica glass walls, coated in Titanium Dioxide, TiO_2 , selectively etched to give an electrode pattern on the surface of

¹Hadron Elektron Ring Anlage, Deutsches Elektronen Synchrotron

the glass. This is done so as to allow the laser light to enter the chamber and to actually ionize the gas inside. The real chambers have copper walls with acid-etched electrodes. This poses no problems for the muons to pass through, but the copper is opaque to light, hence the glass windows.

In Manchester there is only the one such drift chamber whereas at H1 there are 1520 individual chambers which form the large drift planes in a detector known as the Forward Muon Spectrometer.

1.2 The Forward Muon Spectrometer

The purpose of the Forward Muon Spectrometer (or FMS) is to measure high energy muons in the range of polar angles $3^\circ \leq \theta \leq 17^\circ$. The actual spectrometer consists of layers of drift chamber planes, either side of a toroidal magnet.

Eight semicircular steel modules are used in the construction of the toroidal magnet, each with an inner radius of 0.65 m, outer radius of 2.9 m, and thickness of 1.2 m. The field strength varies from 1.5 T at the outer radius to 1.75 T at the inner radius when a current of 150 A is passed through it. This magnet is surrounded by six layers of drift chambers, each of which is made up of eight octants fixed alternately either side of a large aluminium support. This construction gives a small overlap of adjacent octants which means there are no holes, or dead spaces, in the detector through which the muons can pass.

The orientation of the drift cells is such that four of the planes measure the polar angle (θ) providing the momentum of the traversing muon, whilst the remaining two measure the azimuthal angle (ϕ). The theta cells lie tangential to the beam direction, whereas the phi cells are approximately radial within each octant.

The design specifications aimed at measuring muons with momenta in the range 5 GeV to 200 GeV. The lower limit is set by the amount of material the muons have to penetrate and the effect the multiple Coulomb scattering has on the momentum resolution. The expected momentum resolution at 5 GeV is 24% [1], gradually becoming worse until at 200 GeV the momentum resolution is only 36%.

There is a danger of misidentifying the charge of the muons at energies greater than this. Those muons with momenta < 5 GeV will be measured in the forward tracker.

The position of the FMS in the detector is illustrated in the following diagrams, a schematic in figure 1.1, and a cutaway in figure 1.2.

Brief descriptions of the different methods of extraction of the drift velocity, both at H1 and Manchester, are detailed below.

There is no method of direct measurement of the drift velocity for the chambers in H1. It is performed by a method employing a series of checksums [2].

For a real muon track, each x co-ordinate will have a systematic (ϵ_x) and a random (σ_x) error causing a shift of the mean and a spreading of the distribution. The $x - t$ curves are obtained by either using a constant v_{Drift} assumption or fitting with a 4th order polynomial.

The current value used at H1 is $v_{Drift} = 4.77\text{cm}/\mu\text{s}$.

At Manchester, using laser ionization, and exact placement of the ionizing beam, we can calculate the drift velocity from knowing the drift time and the position of the beam. This will allow an actual drift velocity measurement to be obtained which will help the physicists at H1 and provide an independent check of the checksum method. The method also allows a study of the drift-velocity as the electric field and pressure vary. As the gas used here is very similar to the one used at H1, the same trends will be equally applicable to that gas, so the drift-velocity can be modified to account for variation in gas mixture and atmospheric pressure.

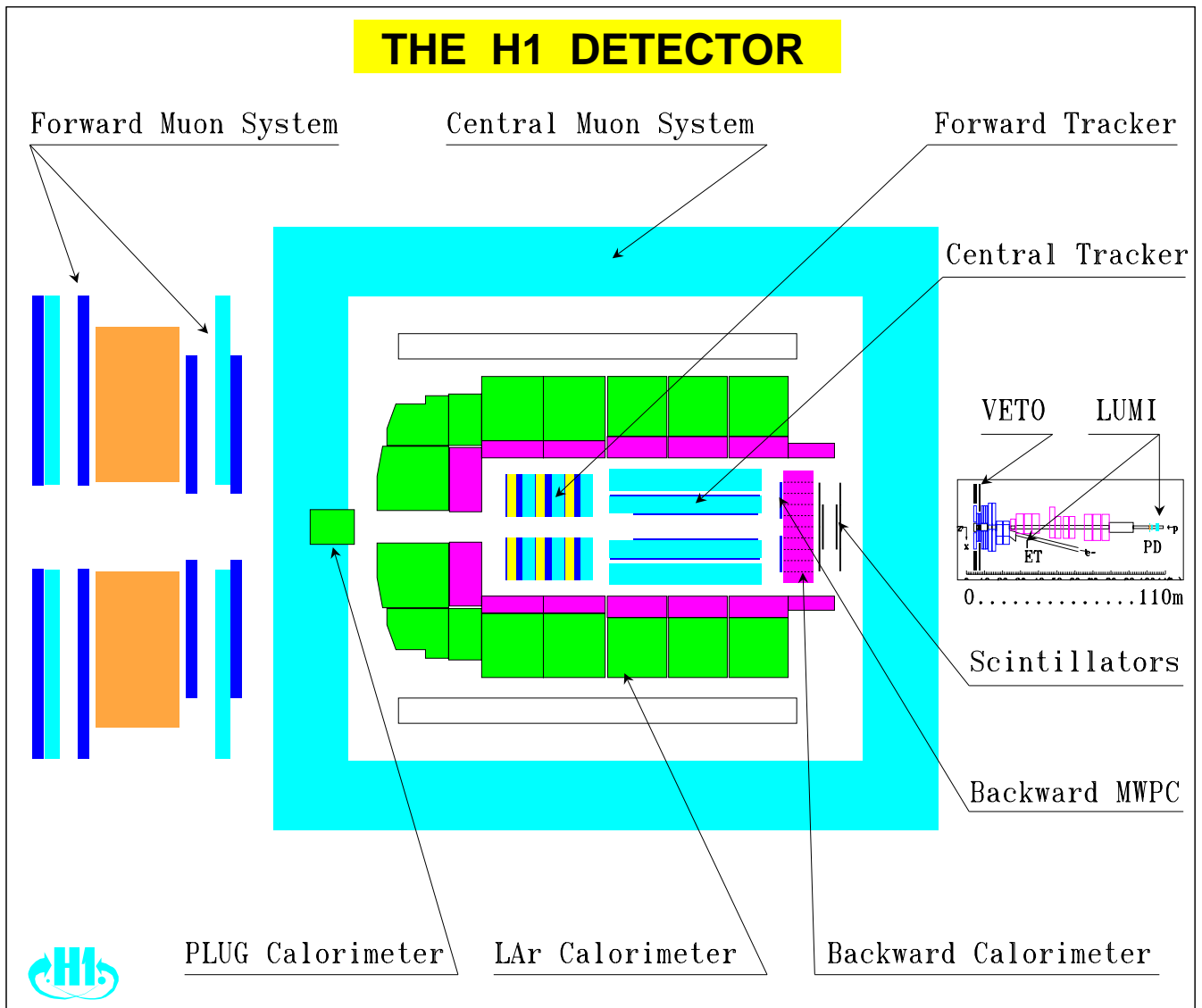
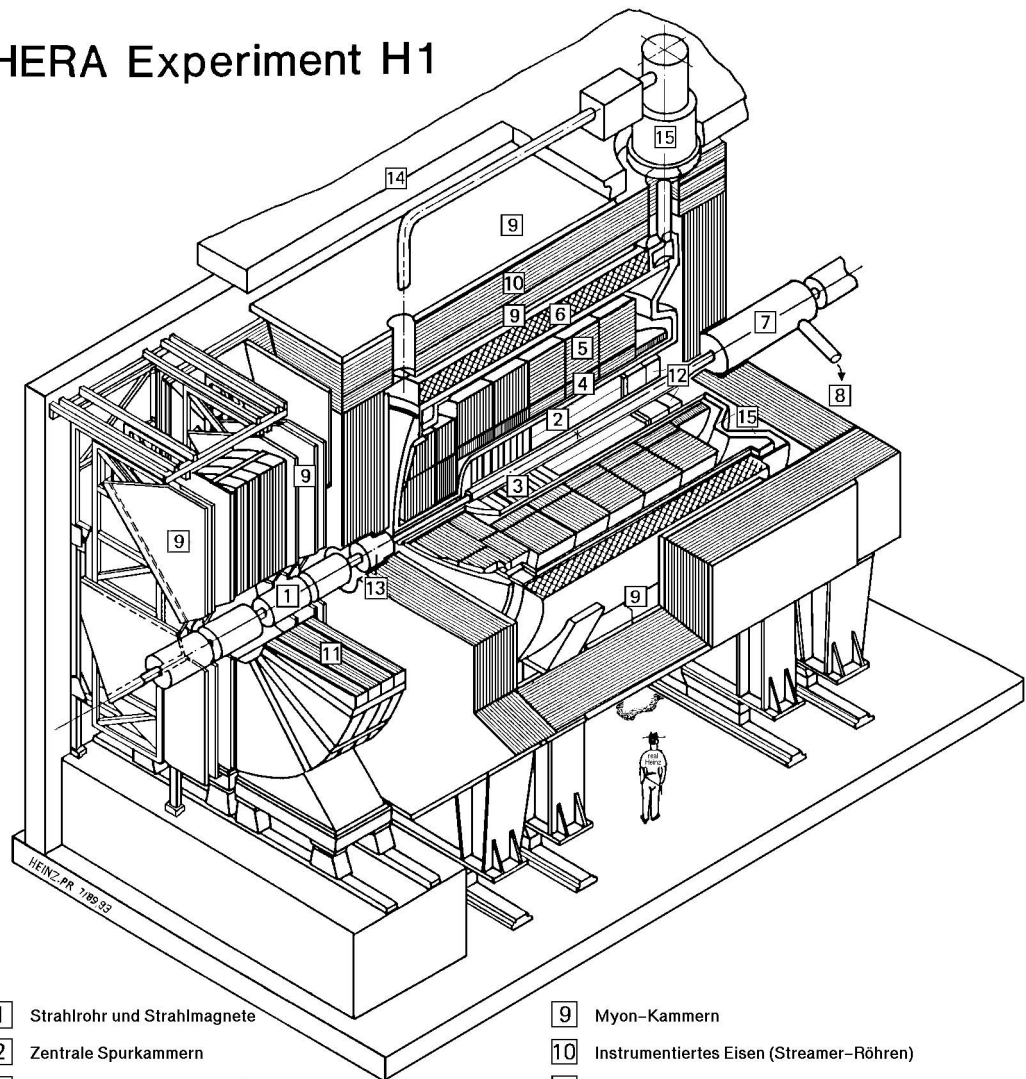


Figure 1.1: A Schematic Of The H1 Detector

HERA Experiment H1



- | | | | |
|---|---|----|--|
| 1 | Strahlrohr und Strahlmagnete | 9 | Myon-Kammern |
| 2 | Zentrale Spurkammern | 10 | Instrumentiertes Eisen (Streamer-Röhren) |
| 3 | Vorwärtsspurkammern und Übergangstrahlungsmodul | 11 | Myon-Toroid-Magnet |
| 4 | Elektromagnetisches Kalorimeter (Blei) | 12 | warmes elektromagnetisches Kalorimeter |
| 5 | Hadronisches Kalorimeter (Edelstahl) | 13 | Vorwärts-Kalorimeter |
| 6 | Supraleitende Spule (1.2T) | 14 | Betonabschirmung |
| 7 | Kompensationsmagnet | 15 | Flüssig Argon Kryostat |
| 8 | Helium Kälteanlage | | |

Figure 1.2: A Cutaway Of The Entire H1 Detector

Chapter 2

The Drift Cell

2.1 Principles And Theory Of Operation

The drift chamber evolved from very early work on the multi-wire proportional chambers, where the possibility of measuring the electrons' drift-time to get information about the spatial co-ordinates of ionizing events was recognized[3].

When a charged particle passes through a chamber, it causes primary ionization of a few atoms of the gas by collisions with the gas molecules. The newly liberated electron will drift in the field toward the sense wire - the ion left behind drifting away from the sense wire. Even though the electron is subjected to a large accelerating potential, it's *average* velocity is constant because it accelerates under the influence of this field, collides with another gas molecule, stops and loses most of its energy, then starts again. The accelerating force provided by the potential difference is matched by the viscous forces experienced during these low energy collisions with the gas molecules along it's path. When the electron gets very close to the central sense wire (a few hundred microns), the electric field becomes very high accelerating the electrons so much that they now have enough kinetic energy to ionize the gas molecules when they collide with them. These *secondary* electrons are themselves accelerated in the field, causing *tertiary* ionization when they, in turn, collide with a molecule. This process, known as avalanching, continues until all the

electrons have moved towards the wire, where they are absorbed, depositing a large charge on the central sense wire, seen as a pulse. The ions move away from the wire, and towards the chamber wall.

The final drift velocity is affected by many external and internal factors such as electric field strength, field direction, temperature and pressure of the gas (affected by atmospheric pressure), composition, stray or external magnetic fields, design of the cell, and any imperfections in its design and construction.

The principle of operation of a drift chamber is elegant in its simplicity. When an ionizing particle, a muon at H1 or a photon in the simulation at Manchester, passes through the gas at a time t_{01} say, and a pulse is detected from the sense wire at a time t say, then we can obtain the drift-time from the difference between these two times, i.e. $(t - t_{01})$. From this we can deduce the spatial position of the traversing particle by measuring the time taken for the ionization charges to reach the wire.

If the drift velocity is not constant across the cell, it is possible to find the spatial distance between the ionization and registration of the event by the formula

$$x = \int_{t_{01}}^t v(t)dt$$

where $v(t)$ is the drift velocity of the electrons inside the chamber. If the drift velocity is constant across the cell, or at least over the duration of the electrons' "journey", then the equation can be simplified to

$$x = v(t - t_{01})$$

This linear approximation, however, is not valid across the whole cell - it is an ideal situation approximation. It is a very good approximation over the middle of the drift distance, but not so good at the extreme edge at the cathode (due to end-effects) and very poor in the high-field region close to the wire. Previous studies [4] have shown that this linear approximation is NOT the case for the drift chamber at H1 (therefore also for the one used in this simulation), as strong evidence for variations of electric field (therefore velocity) across the cell had been found.

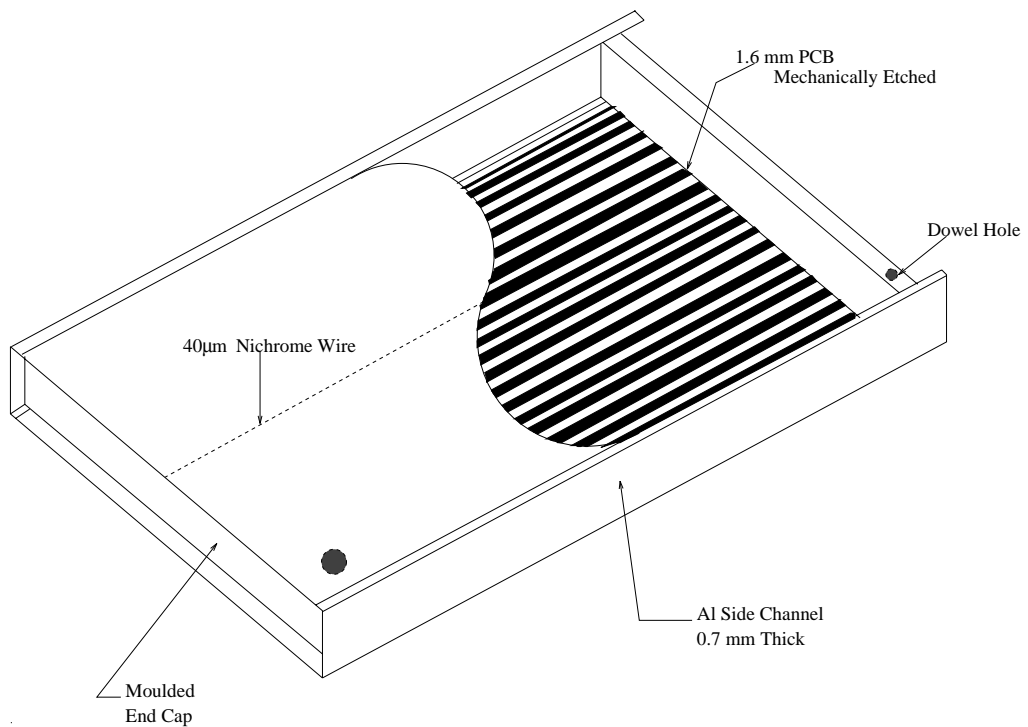


Figure 2.1: A Schematic Of A Drift-Cell

2.1.1 Design Detail

Each cell is comprised of two PCB planes, copper-coated on both sides, and, to minimize the dead space between the cells, 0.7 mm thin extruded Al-profiles. Figure 2.1 shows a schematic of a typical drift cell.

The electrode pattern is better illustrated in figure 2.2.

A nichrome sense wire runs along the cell's major axis, one end of which is connected to a pre-amp, the other to a $330\ \Omega$ resistor and "z-linked" to the adjacent cell. This means that there is only one pre-amp per cell, but effectively both ends of the cell are read out, so the number of channels is halved. The other end contains the high voltage distribution resistor chain and the sense wire readout connector isolated via a 1 nF ceramic disc capacitor. The high voltage is put on the middle strip and passes down along this chain which acts as a potential divider.

This allows both the determination of the track position transverse to the

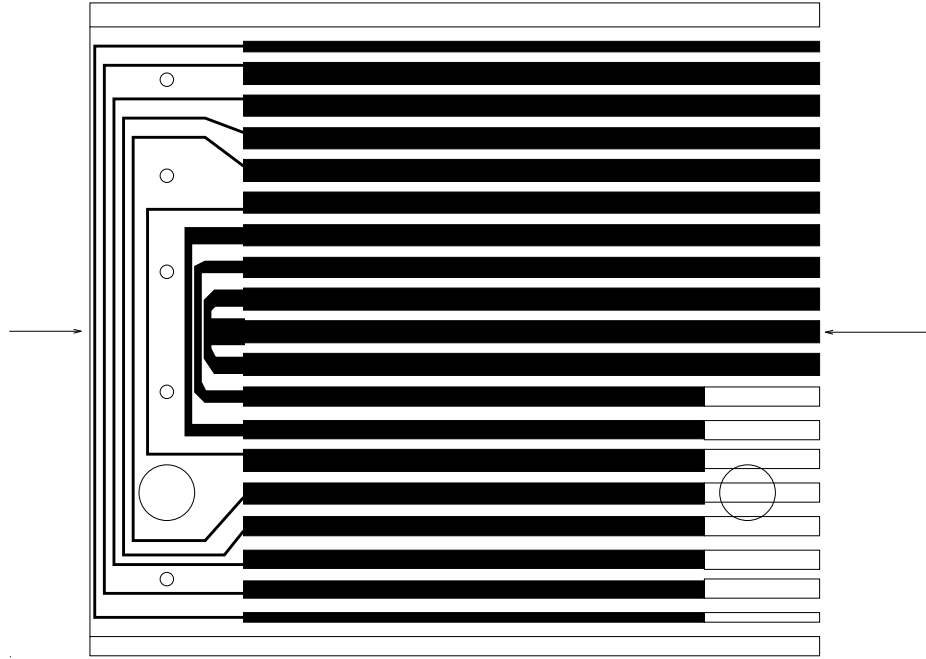


Figure 2.2: The Electrode Pattern

sense wire from the measurement of the drift-time, and also the co-ordinate along the wire by charge division thereby giving information on which cell of a coupled pair was hit.

The voltage applied to the sense wire is 4260 V, and to the central electrode, 2880 V[5]. The 2880 V is passed across a 16 M Ω resistor first, reducing its value to ~ 2663 V. This is the voltage on the central electrode, thus giving an electric field of ~ 444 V/cm throughout the chamber. This field is produced by a chain of nine 20 M Ω resistors, and one 16 M Ω resistor at the end, giving a total resistance in the chain of 196 M Ω . Adding the initial 16 M Ω resistor as well gives a grand total of 212 M Ω .

The value calculated for the total resistance from the current drop at nominal operating voltage is 215.73 M Ω , which is well within the allowed value (212 ± 7 M Ω) if there is a 1% tolerance on each resistor.

2.2 The Gas

The gas used in Manchester is nominally the same composition as that used at H1. The mix may not be *exactly* the same, but variations in the gas composition at H1 are permitted to the first decimal place[6] therefore the drift-velocity measured here will be nearly identical to that at H1. The choice of gas for Manchester was obviously dictated by H1, but the reasons for the choice of this gas were the desire to work in a drift voltage range where there is a plateau in the drift-velocity curve, i.e., it is constant over some range of Electric Field/Pressure ($\frac{E}{p}$), and also that the gas should be very fast - the pulse should arrive in time for the trigger. A non-flammable gas was chosen for extra safety reasons. The current mixture of FMS gas (Forward Muon Spectrometer gas) is 92.5% Ar, 5% CO₂, and 2.5% CH₄. The current cylinder of gas at Manchester comprises of a mixture of 92.83% Ar, 4.60% CO₂, and 2.57% CH₄[7]. The gas is made to flow through the chamber at a rate of about 10 cc/min. A simulation[8] of the variation of drift velocity with $\frac{E}{p}$, for the gas mixture used at H1, is shown in figure 2.3.

As can be seen there is a plateau region where small variations in the electric field and atmospheric pressure should make little difference to the drift velocity.

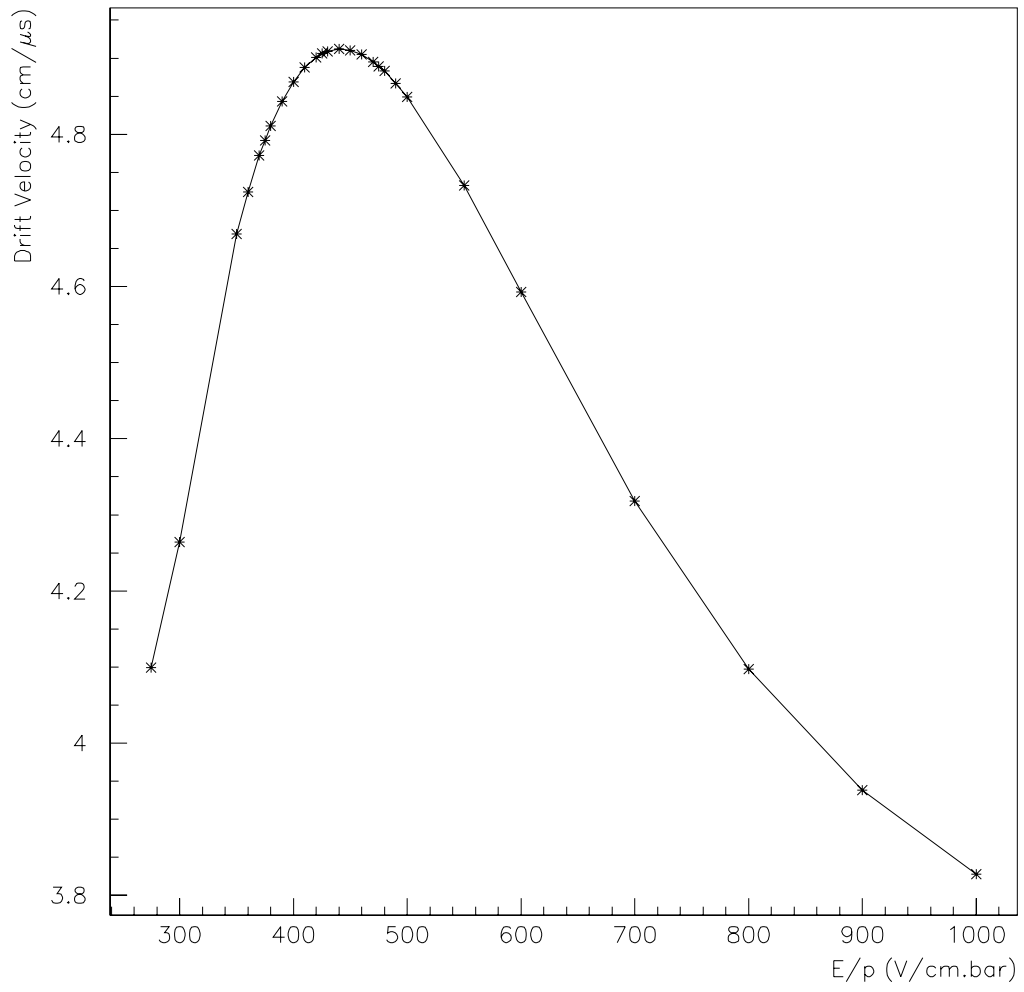


Figure 2.3: Simulation Of Drift-Velocity As It Varies With $\frac{E}{p}$

Chapter 3

The Laser

3.1 Description

Einstein, in 1917, showed that stimulated emission must exist, and within fifty years the first maser¹ was built, leading to the invention of the laser² in 1960 by T.H.Maiman of the Hughes Research Laboratories.

Laser light is distinct from normal light in that it is highly coherent, both spatially and temporally over a long wave-train, it is monochromatic, and it is a highly collimated, intense beam of light.

Figure 3.1 shows what happens, at the atomic level, in a typical laser. A photon of energy \mathcal{E}_{if} interacts with an electron in an excited state, stimulating it to drop to the ground state, emitting another photon in phase with the first, and of the same energy. For this to occur at an useful rate, the electrons must first be forced into the excited state. This is done using a flash-lamp to cause a population inversion, and a pair of highly-silvered mirrors, one at each end of the cavity, to fold the light back in on itself, providing a greater path length. Lasing will only occur if

¹Microwave Amplification by Stimulated Emission of Radiation

²Light Amplification by Stimulated Emission of Radiation

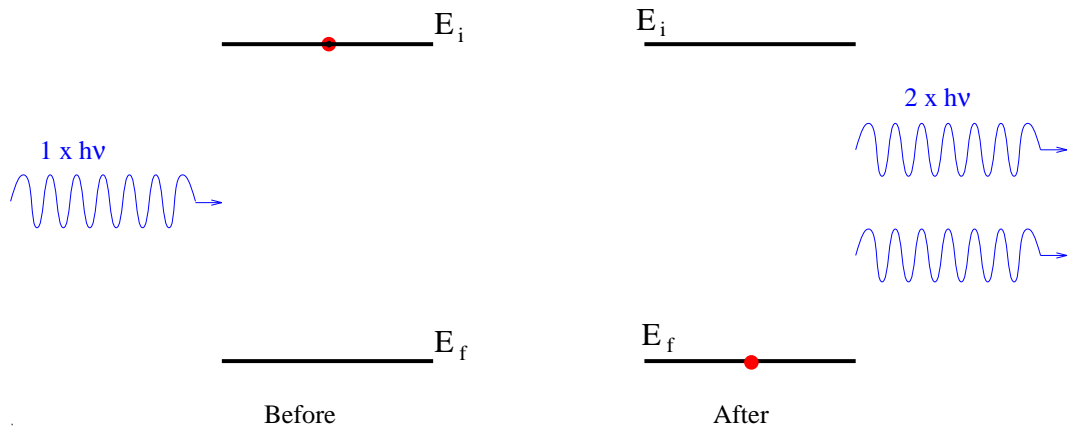


Figure 3.1: Diagram To Illustrate Stimulated Emission

the following criterion is met,

$$\nu = \frac{nc}{2d}$$

i.e., a standing wave in the cavity, where ν is the frequency of the beam, c the speed of light, d the separation of the mirrors, and n is an integer. This ensures the beam's output is monochromatic.

The type of laser used in this experiment is a Nd:YAG laser, but before it's operation can be fully described, an effect known as the Pockels effect must be described.

3.2 The Pockels Effect

This effect is named after Friedrich C. A. Pockels, a German Physicist (1865-1913) who studied it last century in 1893.

The Pockels effect exists only in some crystals that lack a centre of symmetry. These crystals are ones that lack a central point through which every atom can be reflected into an identical atom. Of the 32 crystal classes, 20 of them may exhibit the Pockels effect. It is the same 20 crystals that exhibit the phenomenon of piezoelectricity. Thus all liquids, and many crystals are excluded or forbidden from exhibiting the Pockels effect. The Pockels effect can be summed up by the following

statement:

“...an isotropic substance becomes birefringent when placed in an electric field, \mathbf{E} ...”

Two indices of refraction can be assigned to a crystal, n_{\parallel} , and n_{\perp} , and these are associated with the two orientations of the plane of vibration of the wave - parallel and perpendicular to the applied field. The difference between these, $n_{\parallel} - n_{\perp}$ is called the *birefringence*, Δn .

The Pockels effect is a linear electro-optical effect because the induced birefringence is proportional to the first power of the applied \mathbf{E} -field and therefore to the applied voltage (as opposed to the Kerr effect, a similar effect which is proportional to the square of the field, and is referred to as the quadratic electro-optic effect).

The medium then takes on the characteristics of an uniaxial crystal whose optical axis is the same as the direction of the applied field.

So, drawing on all this knowledge, a *Pockels Cell* can now be described.

3.3 The Pockels Cell

This device is simply an appropriate noncentrosymmetric, correctly oriented, single crystal immersed in a controllable electric field. Such devices can usually be operated at reasonably low voltages ($\sim 5 - 10$ times less than a Kerr (mentioned earlier) cell, would need to do the same job.) They are linear in operation, and are free from toxic liquids (unlike the Kerr cell which contains carbon disulphide or nitrobenzene, a highly toxic and flammable substance.)

The Pockels cell comes in two types, or configurations, known as transverse and longitudinal referring to the alignment of the \mathbf{E} -field with the direction of propagation of the laser beam - transverse is perpendicular, and longitudinal is parallel. The kind used in the Nd:YAG laser is a Brewster angled Pockels Cell in a single mount with dielectric polarizer and compensating block.

Pockels cells have been used as ultra-fast shutters, and as Q-switches³ for lasers. A picture of a Pockels cell can be seen in figure 3.2.

3.4 The Q-Switched Nd:YAG Laser

This is the kind of laser used in this experiment, and is of the class known as “doped insulators”. The active medium in the Nd:YAG is a crystal rod of Yttrium Aluminium Garnet ($Y_3Al_5O_{12}$) doped with a small percentage of Neodymium (Nd^{3+}) ions. The small percentage is typically 0.5% to 2%, and the impurities sit on the lattice at points that would normally be occupied by the Yttrium. The energy level diagram [9] for the transition is shown in figure 3.3.

The most prominent transition emits light with a wavelength of 1064 nm, ($\mathcal{E}_{if} = 1.165$ eV) which is then passed through a frequency doubling crystal, fed back and added non-linearly to the original light-train, and passed through the crystal again, giving a resultant output light of wavelength 355 nm which is in the ultra-violet region. This process is known as frequency tripling. Figure 3.4 [10] shows what happens inside the laser during each firing cycle

The first thing to happen in each laser pulse is that the flash-lamp fires. This must happen in order to cause a population inversion enabling the laser to lase. This firing causes the SYNC out to appear less than 4 μs later. This SYNC out is the trigger to start the Pockels cell charging. The Pockels cell can hold the laser from firing indefinitely (up to $\sim 700 \mu s$), and will do so until the DELAY SYNC output, set by the user, causes the Pockels cell to be armed for discharging. After another delay, set by the user, the Pockels cell discharges, and a laser pulse is emitted from the laser, and detected by the photomultiplier.

³Deliberate displacement or removal of one of the mirrors in the cavity to cease laser action is known as Q-switching. It is also known as Q-spoiling, where the Q is the Quality factor, which is where the name is derived from, as the Q-factor of the cavity is lessened

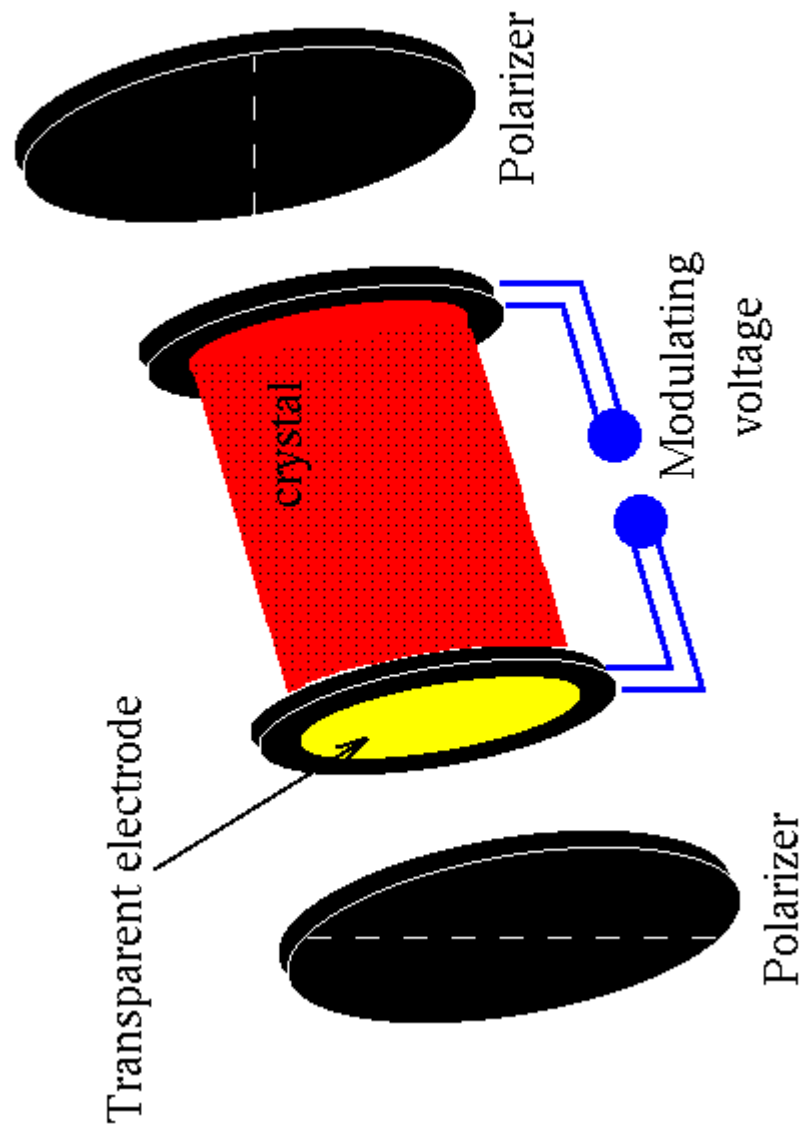


Figure 3.2: A Longitudinal Pockels Cell

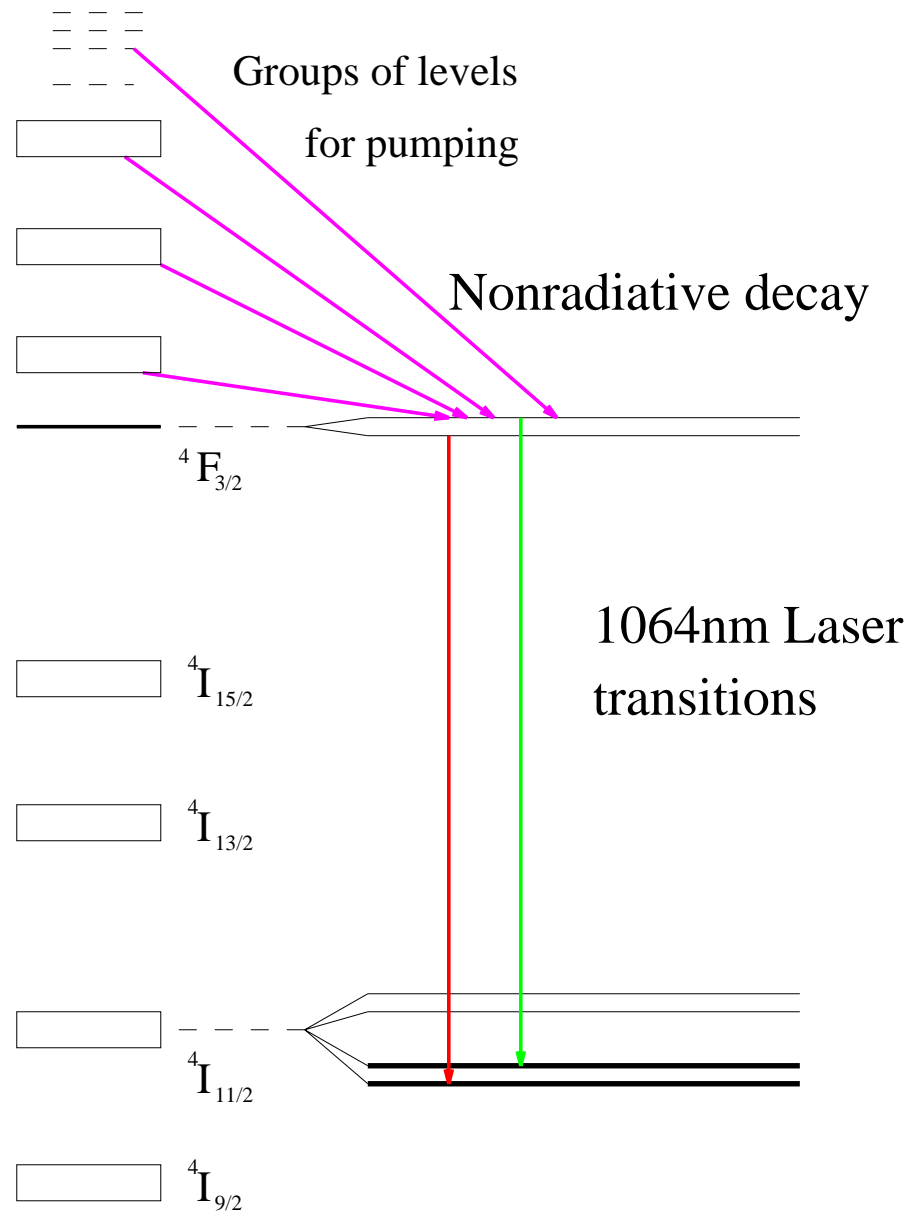


Figure 3.3: Energy Level Diagram For Nd:YAG Laser

Figure 3.4: Illustration Of The Process Of Firing The Laser

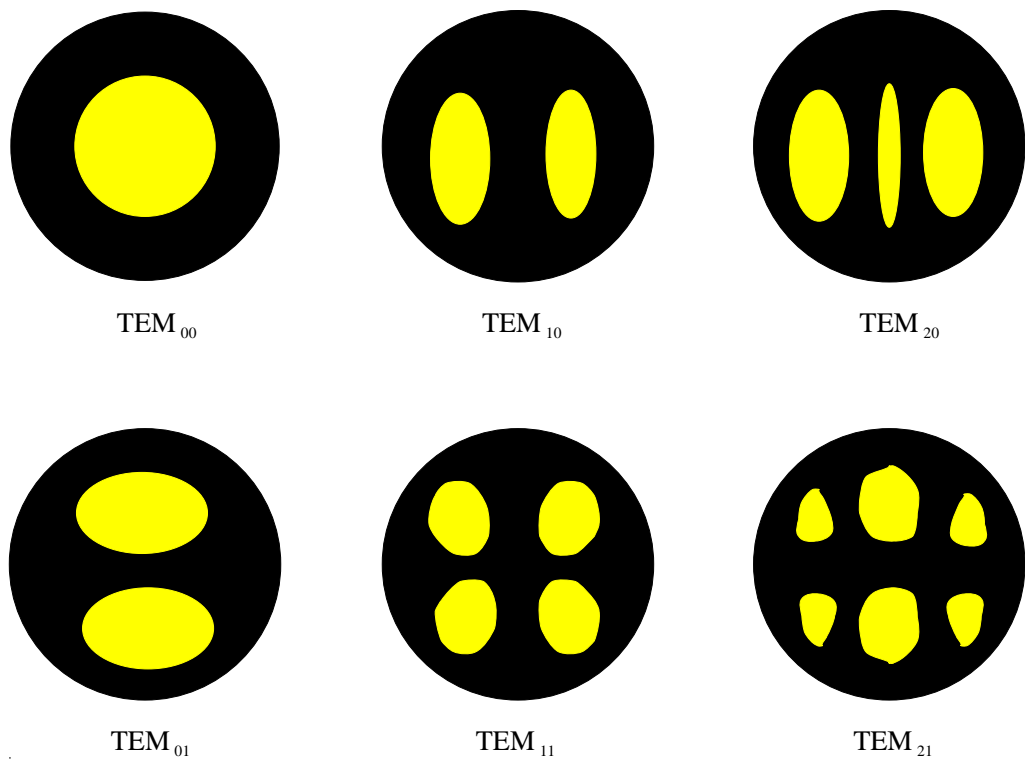


Figure 3.5: Some Beam-Mode Diagrams

3.5 Beam Theory

3.5.1 Modes

Figure 3.5 shows a few possible beam-modes for emission by a laser. They are labelled TEM_{xy} ⁴ where the x and y subscripts are a representation of how segmented the beam is. The TEM_{00} has no cross-sections therefore it is one beam - a Gaussian profile - whereas the TEM_{10} has one line through the beam vertically, giving two spots side by side, but none horizontally, and the TEM_{11} mode has a vertical and horizontal section through it, thus giving four spots.

⁴Transverse Electric Magnetic

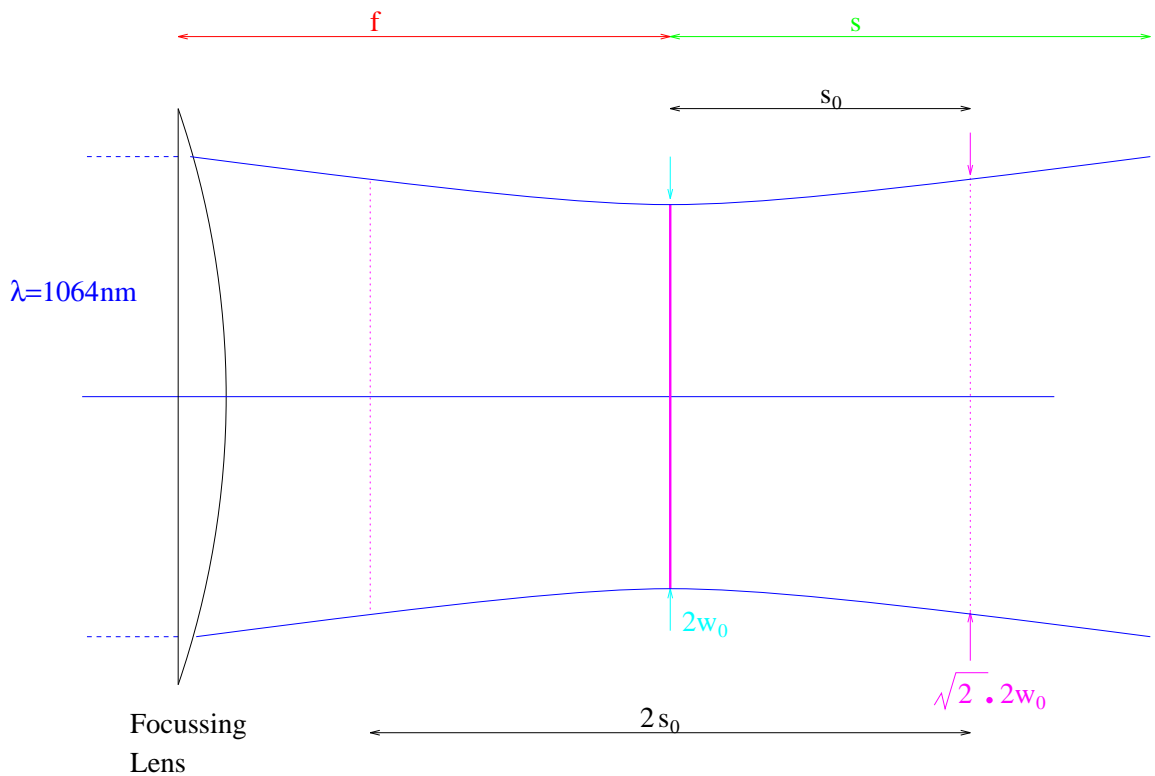


Figure 3.6: A Model Of The Beam Profile As It Nears It's Waist

3.5.2 Waist

As the beam approaches its focus, the spot size is limited to a minimum size called the “waist” of the beam. This waist exists because the mirrors used in the laser cavity are curved, and when this is the case there is a tendency to focus the beam inside the cavity, which gives it a minimum cross-section, or waist, of a certain diameter, $2w_0$. This means that the external divergence of the laser beam is essentially a continuation of the divergence of the waist. To counteract, or attempt to counteract, this problem a system of lenses is placed in the cavity by the manufacturer, Spectron, to defocus the beam back to a parallel beam, so that the exit beam will be a diffraction-limited parallel bundle. Figure 3.6 illustrates the profile of the beam at its waist, where f is the (corrected) focal length of the lens, s_0 the length it takes for the waist to increase in size by a factor of $\sqrt{2}$, $2w_0$ the total width of the beam at the waist, and s the distance at which the waist has doubled in size. Typical values for a Nd:YAG laser are $2s_0 = 8$ m, and $2w_0 = 2$ mm [11].

3.5.3 Focal Length Corrections

The correction to the focal length arises because they are normally quoted at the wavelength of the Sodium D-lines, and as the laser emits light in the ultra-violet the focal lengths will be considerably different. The correction is the following formula[12]

$$f_{uv} = f_{Na_D} \times \frac{(n_{Na_D} - 1)}{(n_{uv} - 1)}$$

and substituting in the numbers[13][14] gives

$$f_{uv} = f_{Na_D} \times \frac{0.45846}{0.47452}$$

or

$$f_{uv} = 0.9661 f_{Na_D}$$

where f is the focal length, n the refractive index, and the subscripts uv and Na_D refer to the ultra-violet and Sodium D-line values respectively.

Chapter 4

Experimental Results

4.1 Experimental Set-Up At Manchester

As can be seen from the following diagram, figure 4.1, the apparatus consists of a laser, a photomultiplier tube, an optical bench with various lenses and filters, and the drift chamber (which is bolted to a stand bolted to the optical table.) The whole set-up is accurately aligned, at least to the alignment accuracies of the chambers at H1, as the experiment is concerned with extremely accurate measurements of both distance and time.

The optical table had been levelled, and verified using a spirit level, after the apparatus had been positioned on it. This had not changed since this was done to set up the experiment initially. The Nd:YAG laser was set up so that the beam enters the drift chamber at normal incidence. The drift chamber is securely bolted to a stand (itself bolted onto the optical table) which can be moved vertically using a micrometer screw gauge, and positioned to an accuracy of $10\ \mu\text{m}$. To focus the beam, a lens is used (a selection is available), positioned on an optical bench, which can be moved in the direction of propagation of the beam, and positioned to an accuracy of 0.5 mm. Another optical bench, closer to the laser, is available for the positioning of a neutral density filter, if required. A Molectron Joulemeter is available, though beam-energy measurements were not required for this investigation.

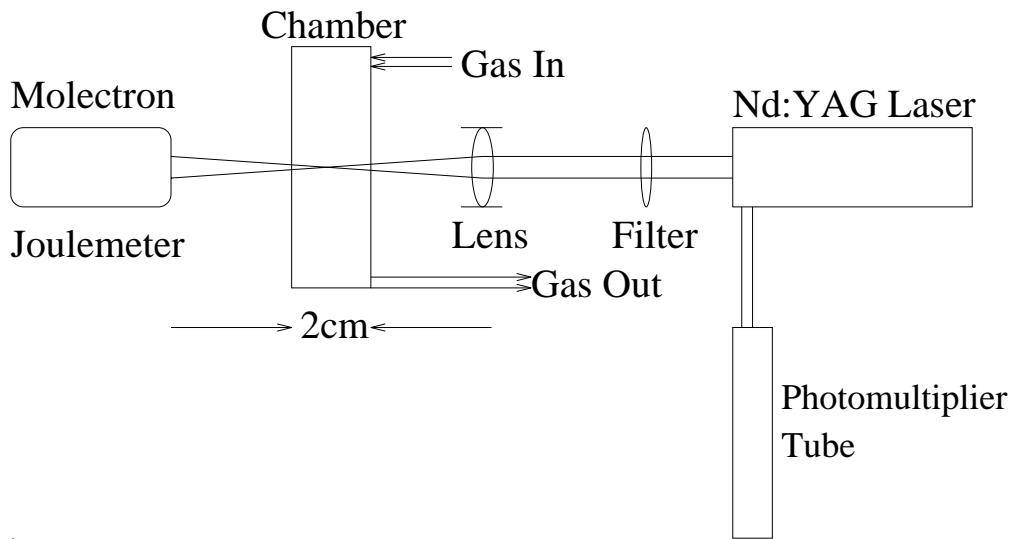


Figure 4.1: Schematic Of The Apparatus

When the laser fires (the processes occurring inside the laser for each firing sequence have been illustrated in figure 3.4) part of the beam is “branched off”, using a beam-splitter, into a photomultiplier tube, which registers the start of an event at a time, t_{01} , in channel zero. The pulse collected on the wire is also fed into the front-end of the amplifier, into channel two, and is called the drift-time, t . Obviously t_{01} happens first, and this goes through a series of discriminators, and a Flash Analogue to Digital Converter (FADC) operating at 100 MHz, and the digitized data appears on screen on an Apple Macintosh II computer running the TestDAQ program¹. The pulse from the sense wire follows a similar path through the electronics and is also stored in the same file. Other channels are not connected, however some RF noise does get into these channels, and they also give a signal in some cases, but it is of no worth, so it is not used in any of the analysis.

4.2 Initial Studies

Preliminary analysis provided some interesting results. What was observed was a main peak in the distribution of $(t-t_{01})$, and also, a smaller satellite peak some

¹Written by Dr. Scott Kolya, H.E.P. Group, Manchester

Simulated Drift-time Distribution using External Test Pulses

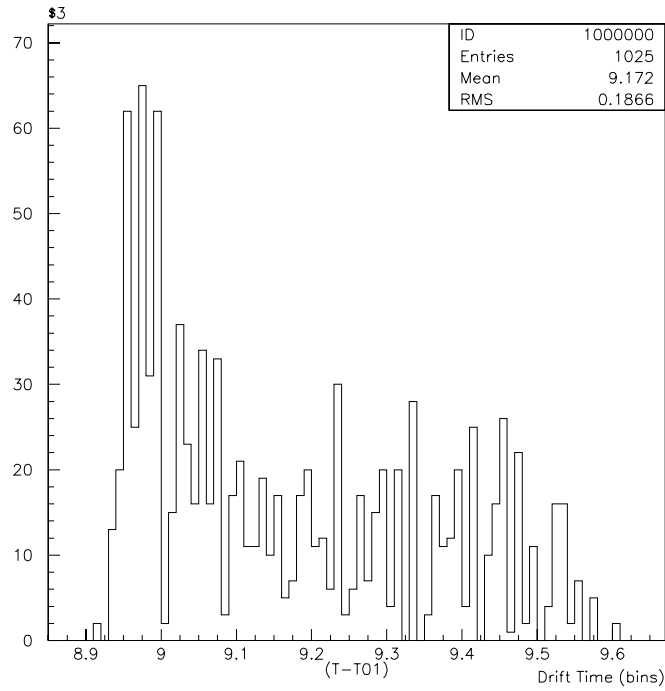


Figure 4.2: Drift-Time Distribution For An Externally-Generated Pulse

30 ns different in time.

At first it was thought to be due to some cable delay, or a “bounced” signal, but this would have required a difference of about 6 m in cable length - which was ruled out. The next explanation thought of was that the satellite peak could be caused by a reflection of the laser beam from some surface. However, this required a single reflection point ~ 4.6 m away (for a direct reflection) - again this was ruled out as being unfeasible, as the room in which the apparatus resides is barely 4 m long. Once these trivial explanations had been eliminated, a more serious problem with the electronics was envisaged, and the circuitry was tested in many ways. A brief outline of the various tests is described below, illustrated in parts with diagrams.

Externally generated pulses were fed down to the front-end along the wires the signal normally comes through, to come back the same way to constitute normal t_{01} and t pulses. The plot obtained is shown in figure 4.2, and no satellite peaks can be seen.

Drift-Time Distribution using Scanner Pulses, threshold 16 decimal

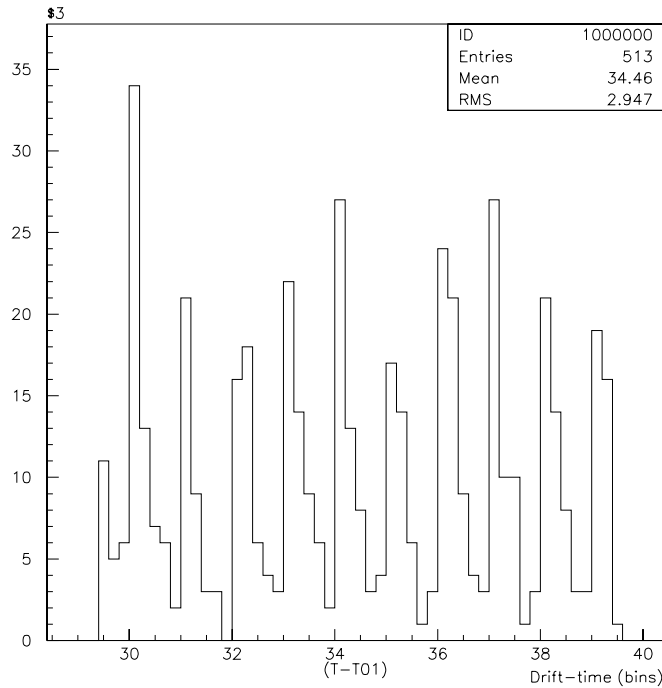


Figure 4.3: Drift-Time Distribution Using Scanner Pulses With Threshold Of 16 Decimal

The next set of pulses used were internally-generated test pulses, generated by the scanner card, instead of a pulse generator, and these, again, follow the same path down to the front-end and back the same way that they came. Figure 4.3 shows the results of this investigation, and, as can be seen, the results obtained showed no indication of a satellite peak.

However, during the taking of this data, a “jitter” was observed on the Macintosh screen, indicating a possible fault on the J_0 card in the back of the scanner. This card was swapped for another, and the same investigations performed again.

It was soon discovered that the jitter was still apparent therefore the original J_0 card was put back as it was not faulty. The jitter, because it is observed in all channels, will cancel in the subtraction of one channel from another.

The scanner card itself was then swapped to see if different results would

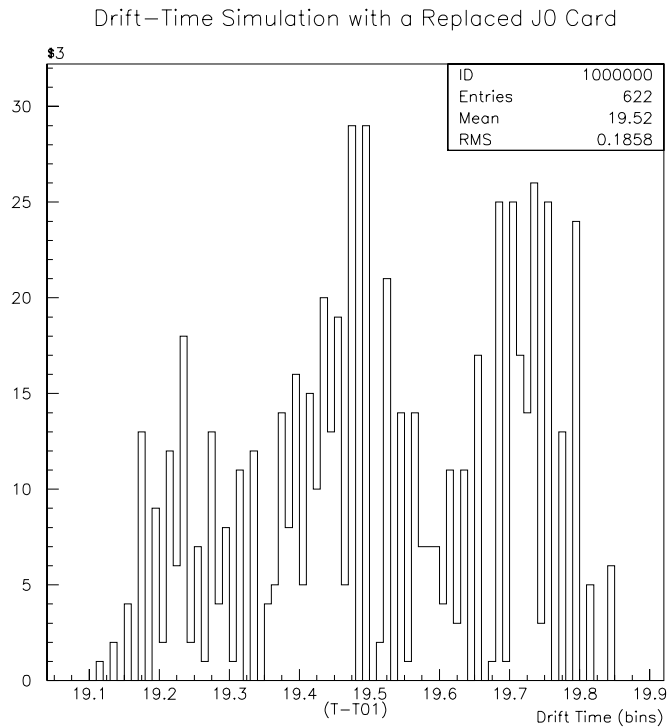


Figure 4.4: Simulated Drift-Time Distribution With A New J₀ Card

be seen, but, no satellite peaks were seen in the distribution, although the jitter, still apparent, was explained as there being no reference clock to start the timing, so the placement on screen, say, of a t_{01} pulse is arbitrary within a window of about 100 ns. As mentioned earlier, it is the difference between t and t_{01} which is important, and no “jitter” or satellite peaks appear in this distribution.

Now that a different card was in place, a run performed entirely on test-pulses was performed (generated by the scanner), without a PMT pulse in channel zero, whereas before the pulse in channel zero was generated from the PMT by the laser. The graph obtained is shown in figure 4.4.

The final graph, figure 4.5, is a purely internally-generated pulse, and there is NO 30 ns satellite peak, effectively proving that the electronics are not at fault.

The next step was the dismantling of the chamber and putting externally generated time pulses actually into the front-end instead of the outside connections. Both FADC channels (0 & 2) needed to be changed, though an adapter was also

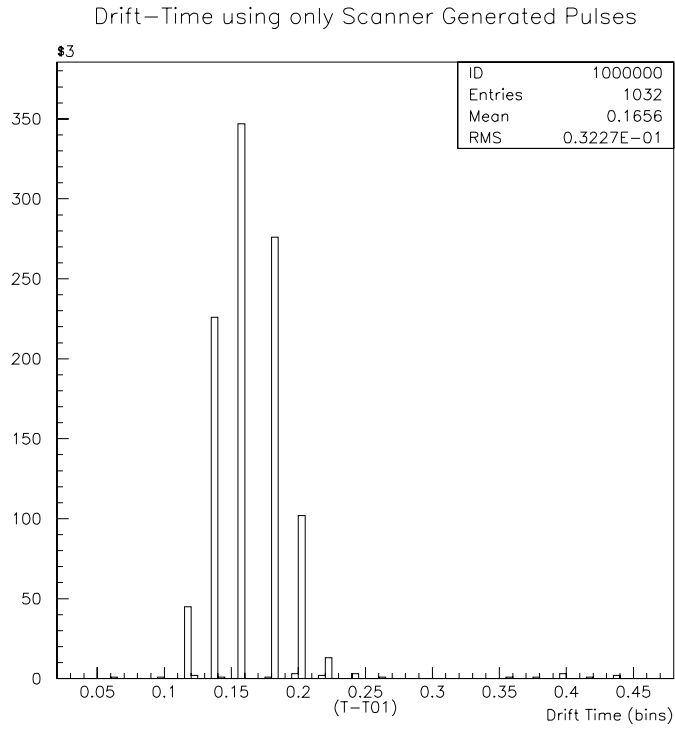


Figure 4.5: Drift-time Distribution For Wholly Scanner-Generated Pulses

fitted to make it a little easier to get at the links in the future. The results showed no indication of a satellite peak, and this is demonstrated in figure 4.6.

It was then decided to put these pulses in every channel apart from zero, where we would use an actual laser pulse from the PMT. Again, no satellite peaks were seen.

The next thing done was to use the PMT pulse as a start signal, feed it through the discriminator, take it back down to the front-end, and also use it as a stop pulse, at time t . This is shown in figure 4.7, and again, as expected, no satellites can be seen.

It was decided to take some more “real” (as opposed to simulated) data, by using channels four and six instead of zero and two, to see if the problem remained. Both these channels were susceptible to noise, or ringing, from the laser, but the satellite peaks were still in evidence proving that channels zero and two were not to blame in the creation of the satellite peak.

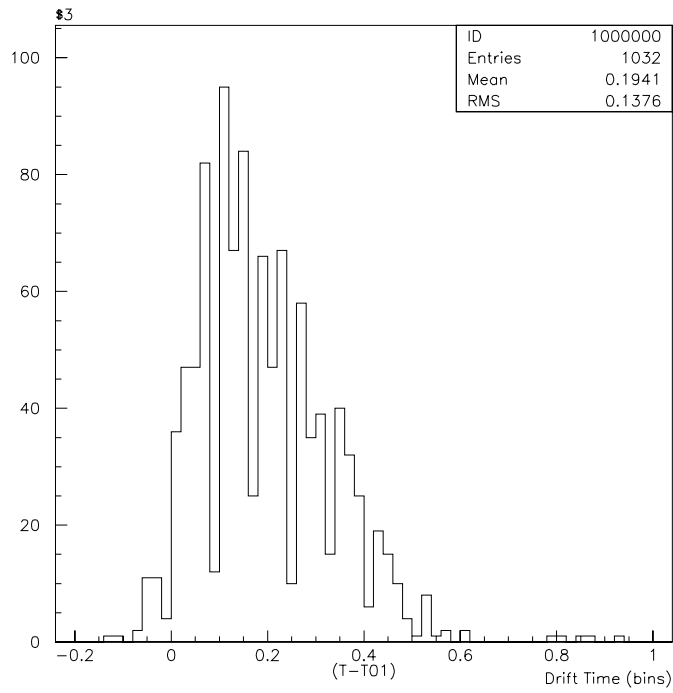


Figure 4.6: Direct-Input Externally Generated Pulses

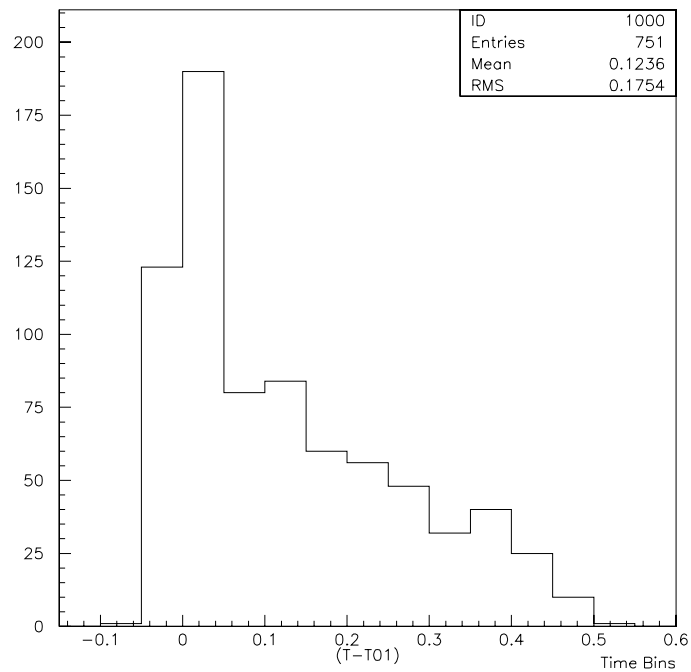


Figure 4.7: Using The PMT Pulse As Start And Stop

4.3 Alignment

Even though it was believed that a slight misalignment of the beam could not cause these satellite peaks, the alignment was checked just to be thorough in the investigation. It was found that the beam-centre dropped by ~ 2 mm over a distance of ~ 2 m, and this was corrected, so that no detectable drop occurred. A slight left-right misalignment, introduced by the correction of the vertical alignment, was corrected and the beam was parallel to the optical bench once more, striking the chamber wall at normal incidence.

4.3.1 Finding The Middle Of The Cell

This can be done by moving the point of focus “through” the cell, to see if a minimum drift-time can be found, which would correspond to the middle, as the electrons have a shorter path to drift to the wire than those at the walls of the cell. Before this could be done, however, some measurements had to be taken in order to relate the actual distance the centre of the lens is from the cell with the marker distance on the scale.

As can be seen from figure 4.8, measurements of the “gap”, the holder width, the plastic width, the lens width, and the distance between the holder and the lens, called the offset, had to be taken, and the following formula relates the actual reading, called scale, to the focal distance meaning that the chamber wall lies at

$$\text{Scale} + \text{Gap} - \text{Plastic Width} - \text{Offset} - \frac{1}{2}(\text{Lens Width})$$

from the centre of focus.

Because so many measurements had to be taken, the accuracy of the final result is adversely affected, giving the centre of the cell at 78 ± 5 mm.

Figure 4.9 is a plot of the drift-time against “scale” - the uncorrected lens

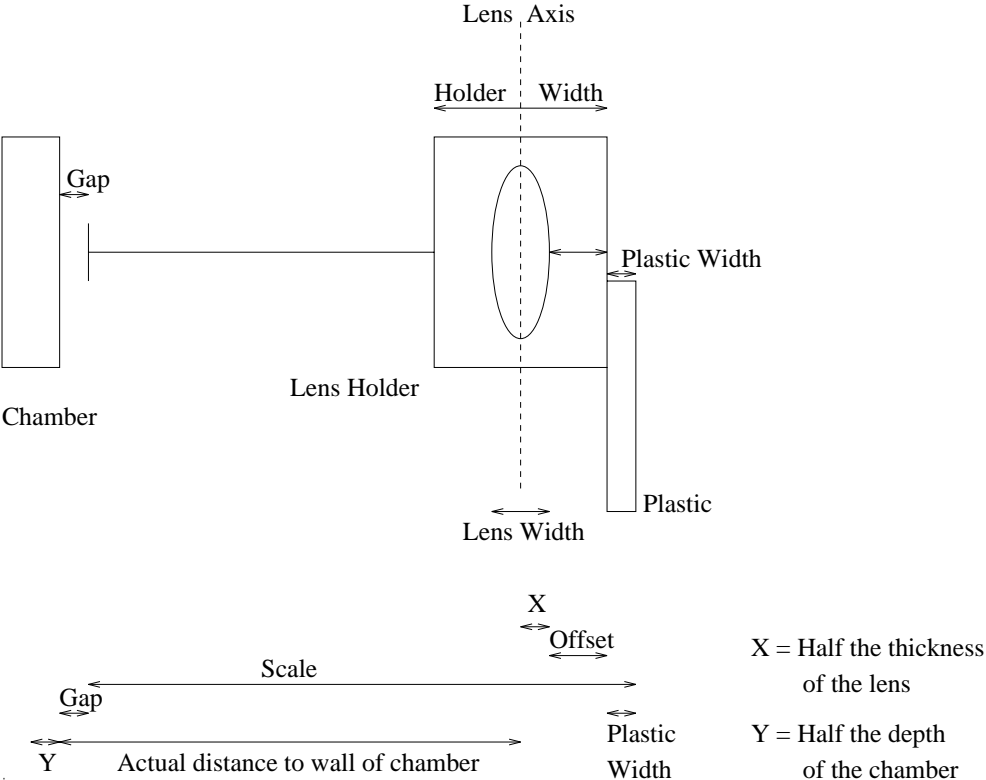


Figure 4.8: Illustration Of The Measuring Method And How It's Related To The Actual Distance

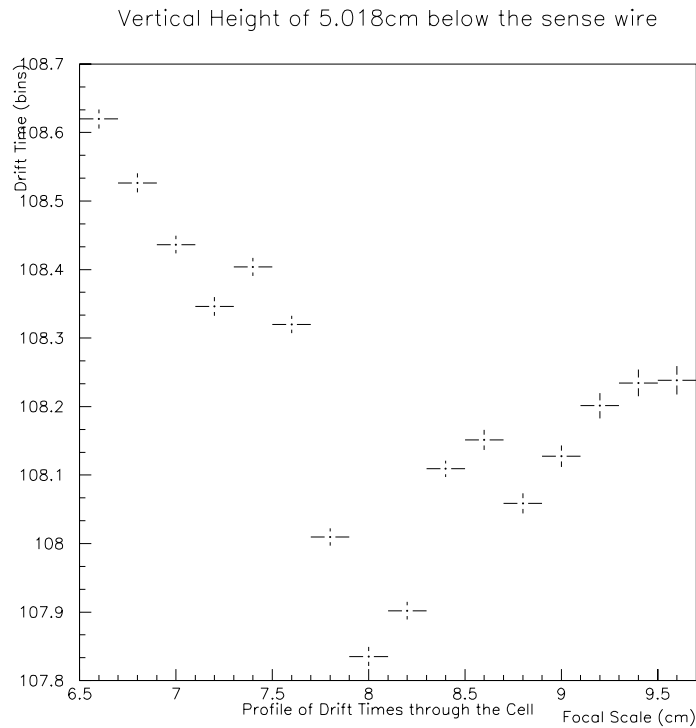


Figure 4.9: Variation Of Drift Time With “Scale” Through The Depth Of The Cell

position. It can be seen that there is a noticeable (though small) dip at ~ 7.9 cm which confirms our theory, and agrees well with the calculation. Once the centre of the cell had been found, measurements could be made of the drift times at different vertical positions in the chamber.

4.3.2 Where To Take The Data

As has already been mentioned in earlier chapters, the drift cell has 4 mm wide Titanium Dioxide (TiO_2) strips on the surface of the glass to act as electrodes, and it was hoped to be able to take data through these, as well as in the gaps between them. However, TiO_2 is a highly efficient photoelectric emitter in the ultra-violet, and this completely dominates the signal in the data taken through them. It is for this reason that no more data were taken through the electrodes, and the gaps were concentrated on. Finally, once the data are written to the hard drive on the Apple Macintosh, it can then be sent to the Dec Alpha workstations (running Open VMS)

for analysis - see chapter 5

4.4 Investigation Of The Laser's Properties

As mentioned earlier in this chapter, early work on the calibration and setup of the experiment provided some interesting profiles in the plots of the drift time, $(t-t_{01})$. What was expected was a sharp "spike" a time-bin wide in the $(t-t_{01})$ distribution (for that particular channel). However, a satellite peak was observed at ~ 30 ns later than the main peak, and about a tenth of the height.

4.4.1 Laser Intensity

In investigations to find the ideal voltage for operation it was noticed that the higher the laser voltage, then the worse the 30 ns gaps became - i.e. more apparent. It was also noticed that as the wire was approached, the satellite peaks became more apparent, and also more of them appeared, clustered around the main peak at ± 30 ns and also at ± 60 ns, i.e., on BOTH sides of the main peak, not just at +30 ns as was previously observed. Data were then taken at various laser voltages from 700 V to 750 V, primarily to find some kind of link between the satellites and the voltage, but also because the laser could run for longer at a lower voltage without overheating². The data obtained for 730 V and 750 V are illustrated in figures 4.10 and 4.11 and, using these data, and others at different voltages, it was possible to construct a graph illustrating the height of the pulse against the voltage of the laser (figure 4.12). The mean heights must be below 1000 on the scale used in the DCTEST analysis program (see chapter 5) - otherwise they give false results - and this can be seen for the point at 750V - it does not lie on the curve. The curve is most definitely a parabola, or second order polynomial, which indicates that, as is expected[15], the ionization is a two-stage, or two-photon process. The curve should be parabolic with the intensity of the beam, but, as the precise relationship between

²When the laser becomes too hot, it automatically cuts out, and it has to be left to cool before being switched back on again. This problem was eventually relieved when a hole was cut in the wall behind the heat exhaust of the laser

the intensity and the voltage is unknown, then a plot of the height against voltage is the best that can be shown.

It was decided that, from then on, the laser should be run at 730 V and at a repetition rate of 5 Hz, as this was where the best trade-off between small satellites and large main pulses was found to occur, and also because the laser seemed to operate efficiently without overheating.

4.4.2 Beam-Shape Investigation

Once all the electronics had been thoroughly tested and found blameless, the inescapable conclusion was that the laser was at fault, and that instead of a Gaussian beam profile (TEM_{00}) we were actually getting a TEM_{11} profile where the separation between the beams was of the order of 1 millimetre, therefore it was decided to investigate the shape of the beam and the focal region using a device called a Reticon array³, a 6.4 mm long strip of 256 charged-couple devices - each a 25 μm square of silicon. The photodiode array, or Reticon, was mounted in such a way that we could measure the altitude of the centre of the beam (see figure 4.13.) Provided the beam remains parallel to the optical bench at a certain height above it, the centre should remain on target no matter how divergent it becomes. It was found in other investigations (see above) that the “best-looking” pulses appeared at a laser voltage setting of 730 V at a repetition rate of 5 Hz. The investigations of beam structure were performed at this setting.

As can be seen from the diagram, the array can be moved backwards and forwards through the waist of the beam, and also vertically through it.

It was found that there was only one major spot at the focus, but with small “shoulders” when not focussed properly. Spot-size at the waist is around 70 μm , which is very much smaller than the resolution of the drift cell. This is with a 25 mm lens, but it is expected[16] that the spot-size of the 100 mm lens is not much bigger, and should still be less than the resolution of the cell.

³kindly loaned by Dr. Lawrie Gloster, LINAC

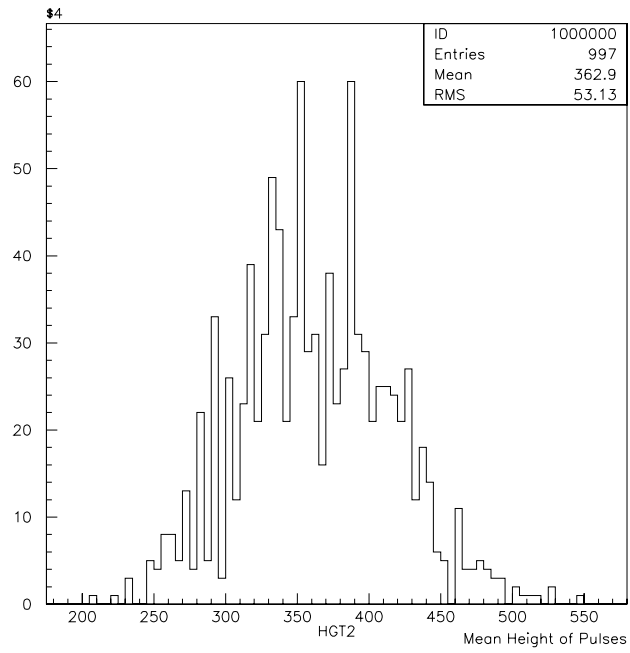


Figure 4.10: Heights Of Pulses At 730 Volts

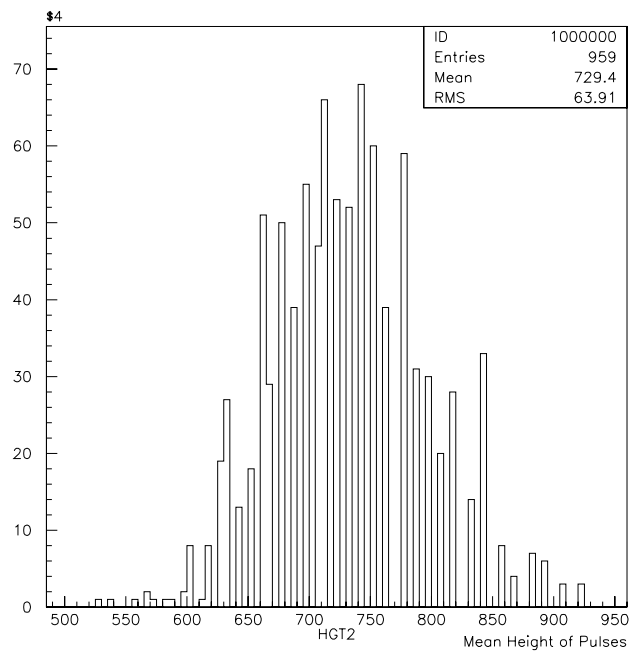


Figure 4.11: Heights Of Pulses At 750 Volts

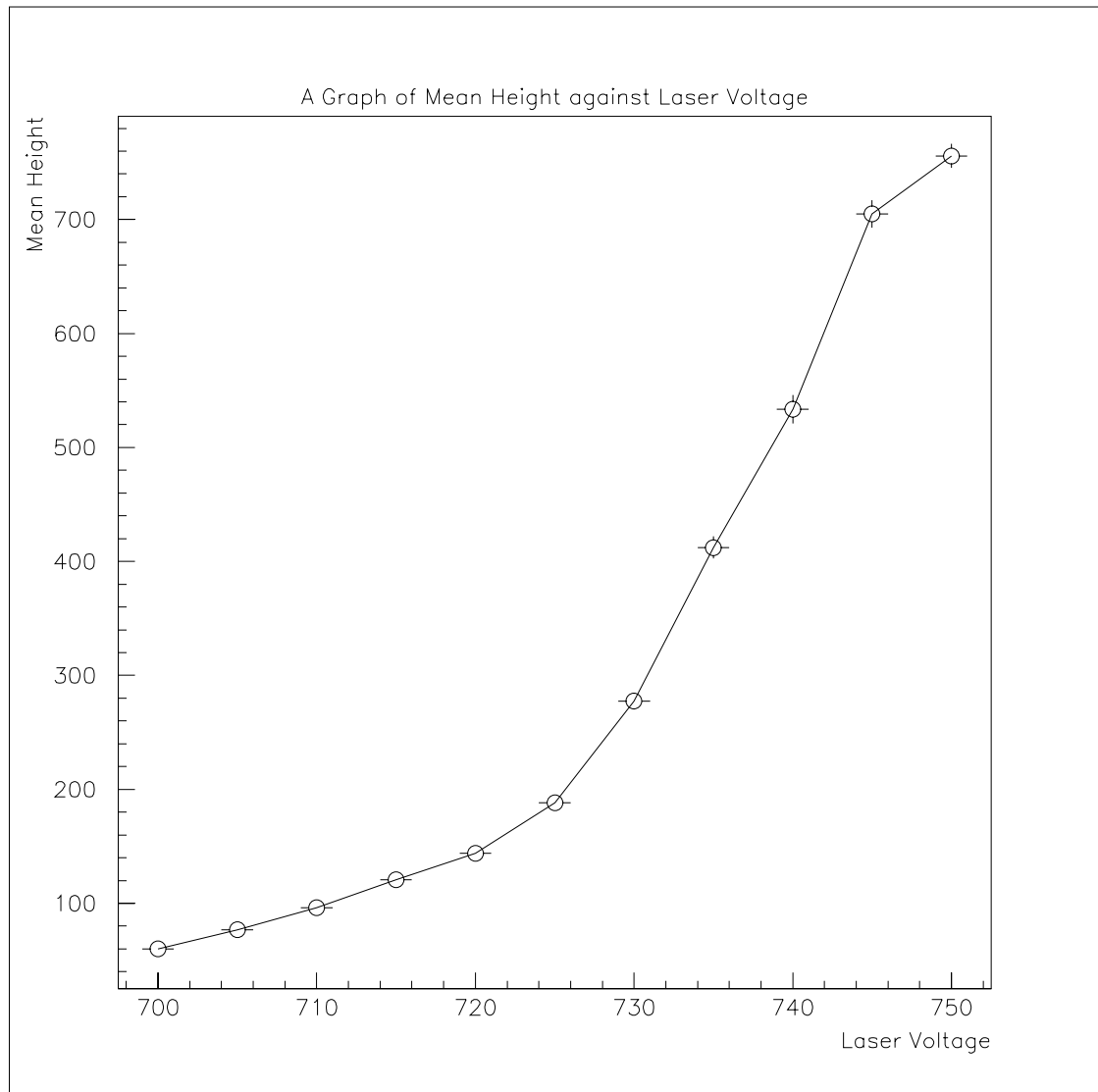


Figure 4.12: Parabolic Nature Of The Laser Pulse Heights Against Voltage graph

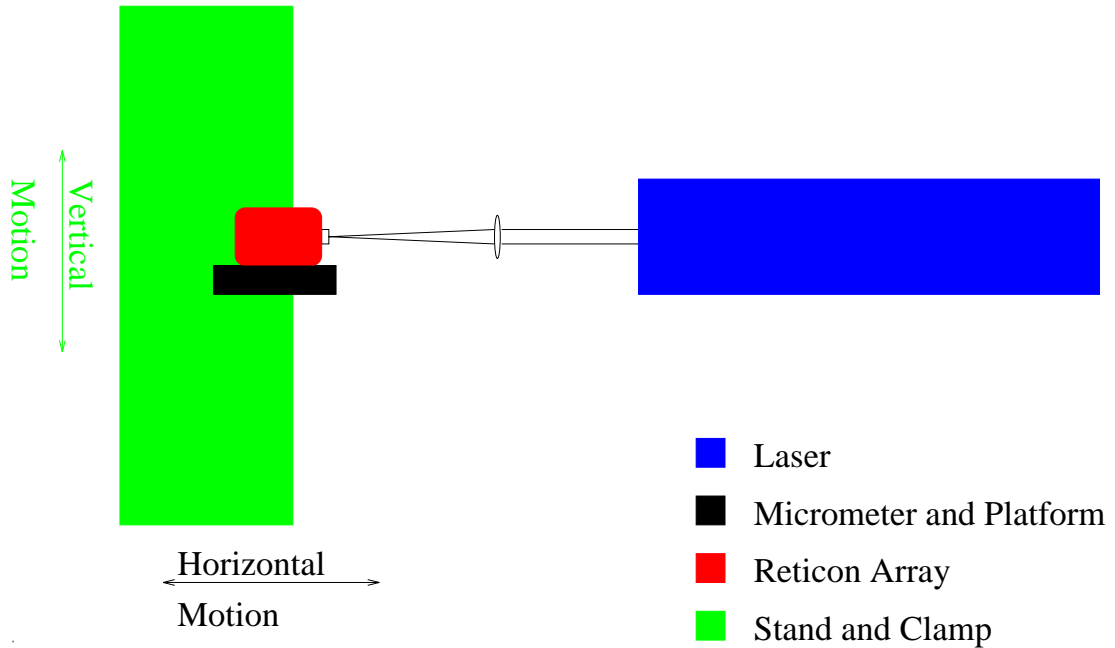


Figure 4.13: The Reticon Array Set-Up

4.5 Time Binning Investigation

The scanner cards both at Manchester and H1 have internal crystal clocks in them which regulate their operation. The Manchester clock frequency is 100.00000 Mhz, whereas the one at H1 is ~ 104.09727 MHz. This means that the time-bins (the reciprocal of these frequencies) are 10 ns and 9.6064 ns respectively. This investigation was performed to see if the width of the bin could be determined experimentally. This was done by feeding a signal into one channel, zero, then delaying it by a known amount, and feeding that into the next channel, two. Delay cabling of value 900 ns in total were used, with the extra connecting cables adding a further ~ 60 ns. This could be checked on the Hewlett Packard Digitizing Oscilloscope.

A “long” run was taken so that the average delay over 1024 scope measurements could be found. The value obtained for the delay in this way was 959.262 ns. This gave an useful data sample of 1411 events (the discrepancy arises due to the scope sampling at a slower rate than the data were generated).

Knowing the time between the t and t_{01} exactly, it is possible to deduce

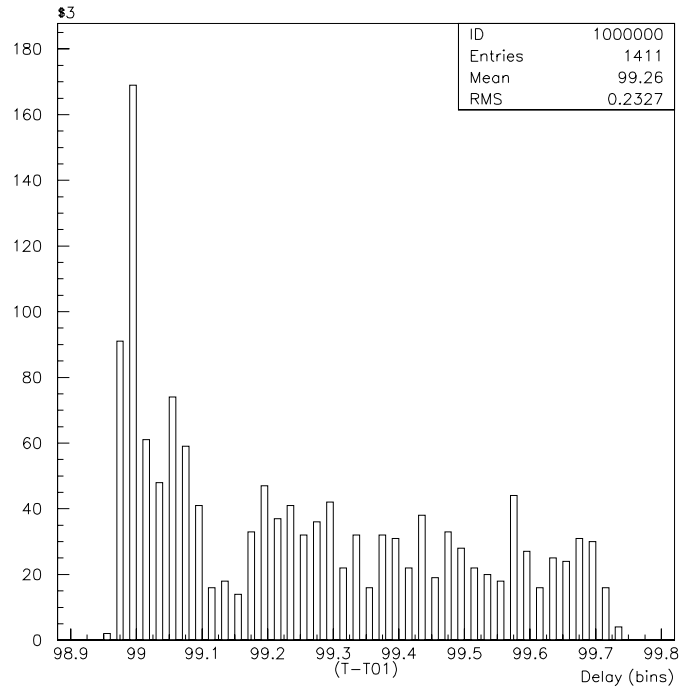


Figure 4.14: Illustration Of The Time-Binning Investigation

the bin width from the PAW⁴ plots, once the raw data have been fed through the QT algorithm in a program called DCTEST. Figure 4.14 is the graph obtained from these data.

The PAW program gave a mean “drift-time”, or delay, ($t - t_{01}$) of 99.260 ± 0.006 bins, meaning that each bin is

$$\frac{959.262}{99.260} \text{ ns wide} = 9.664 \pm 0.001 \text{ ns/bin}$$

There exists a facility for checking the output of the clock from the front of the scanner card. The clock frequency is divided by 10 to give the HERA clock speed, and this can be checked on the scope, and this gave a frequency of 10.00 MHz exactly - i.e. a clock speed of 100.00 MHz exactly. This is a curious result, and the only explanation that can be given is that there exists some internal (unmeasurable) delay between signal input and output. The crystal itself, which governs the rate at which the FADC works, gives a bin-width of 10 ns exactly, and not, as determined

⁴Physics Analysis Workstation

by experiment, 9.664 ns.

Chapter 5

Analysis

5.1 Introduction

As mentioned in chapter 4, the Data Acquisition Program, TestDAQ, actually gathers the data, and writes it to a file in a way in which the DCTEST¹ program can understand. The files are transferred electronically, over Ethernet, from the Apple Macintosh to the Dec Alpha workstations, where the DCTEST program has been compiled, and can be run. Before it can be run, however, a file called DCTEST.TXT¹ must be edited to include all the files that need to be analysed. This file is where the DCTEST program looks to find out how many “runs” there are in the file to be analysed, and reads in the (up to) three run-dependent parameters, chosen and entered by the user. The parameters chosen for most of these files are RNP1: Vertical height of chamber; RNP2: Scale reading; RNP3: Atmospheric pressure (not actually used in the drift-velocity extraction, but useful for compiling the curve of drift-velocity against $\frac{E}{p}$.)

Once this has been done, the DCTEST program can be run. The time and charge information is obtained solely from the rising edge and peak region of a pulse. The program looks for two successively rising digitizings above threshold, which it calls a pulse start, and assigns the end of that pulse eight time bins later or when

¹written by Dr. J.M.Foster, H.E.P. Group, Manchester

it encounters the second of two successively falling digitizings below threshold after the peak. The QT algorithm within DCTEST then assigns an “arrival time” to the pulse obtained by fitting a line to the steepest part of the leading edge back to the intercept with the ground level, or some other previously defined (in DCTEST.TXT) level, normally some fraction of the maximum height of the pulse. The DCTEST programme then collates the data in the file creating a file called an NTUPLE.

5.2 Ntuples

An ntuple can be thought of as a histogram of histograms. Every “event” in the file is made into a histogram, and the ntuple is an overall histogram of all the individual histograms. It is needed in this ntuple form so that the Physics Analysis Workstation (PAW) program can use it. Once the DCTEST program has read all the raw data (from the R****.MAC file) and written the DCTEST****.NTUPLE file, it will be loaded up, on entry into PAW, as ntuple identifier 100, in logical unit number 1. It is now possible to plot any of the quantities listed in table 5.1 against any other, or combinations of any other, to produce illuminating answers.

NTUPLE ID= 100 ENTRIES= 5181 Detector Test

Var numb	Name	Lower	Upper
1	IRUN	0.318900E+04	0.319300E+04
2	IEV	0.200000E+01	0.521000E+03
3	IBL	0.100000E+01	0.300000E+01
4	IHIT	0.100000E+01	0.300000E+01
5	FADC	0.000000E+00	0.200000E+01
6	T	-.380000E+01	0.175100E+03
7	TD	0.000000E+00	0.000000E+00
8	Q1	0.000000E+00	0.790000E+02
9	Q2	0.000000E+00	0.450100E+04
10	RT1	0.000000E+00	0.200000E+01
11	RT2	0.000000E+00	0.120000E+02
12	HLEN	0.300000E+01	0.150000E+02
13	T01	0.000000E+00	0.145200E+02
14	HGT1	0.000000E+00	0.246600E+02
15	HGT2	0.000000E+00	0.100818E+04
16	PED1	0.000000E+00	0.103000E+02
17	PED2	0.000000E+00	0.323200E+02
18	RNP1	0.245610E+02	0.263610E+02
19	RNP2	0.780000E+01	0.780000E+01
20	RNP3	0.100700E+04	0.100700E+04

Table 5.1: A Table Of PAW Parameters

As can be seen from table 5.1 there are 20 parameters available to choose from, however, not all of which are relevant to this experiment. The parameters used constantly or regularly are the following:

IRUN - Simply an integer recording the Run Number.

IEV - This is the EVENT number, and records the number of events in each RUN

IBL - This is the number of the data block within the data bank, where there is one data bank per event

IHIT - This records how many HITS there are per block.

FADC - This keeps a record of how many data channels from the Flash Analogue-to-Digital Converter there are and what exactly is in each channel.

T - This is the time at which the Drift Pulse is recorded.

Q2 - This is the integrated charge of a pulse

HLEN - This is called the Hit Length, and records how LONG each pulse is in every IHIT selection.

T01 - The START time, as taken by the Photomultiplier tube.

HGT2 - This records the HEIGHT of each pulse in FADC units.

RNP1 - User-configurable parameter, set to the vertical chamber height.

RNP2 - User-configurable parameter, set to the scale position of the lens.

RNP3 - User-configurable parameter, set to the atmospheric pressure.

The first version of the DCTEST program only allowed single runs to be analysed at a time, but, modifications allowing many separate runs to be included in the same file (using the append mode in the TestDAQ program) mean that all the data are collated into the one ntuple, and if a particular run needs to be analysed, then its run number (IRUN) or parameters (RNP1,2,3) can be specified to be picked

out from the whole sample.

As we are interested in a value for the drift-time, it is sensible to obtain a plot, or histogram, of the $(t - t_{01})$ distribution. This can be done in PAW. To illustrate how the cuts selection is arrived at, plots of the various stages in the selection are included. Figure 5.1 shows an uncut distribution.

In this particular data sample, the events are collected into one file from runs at different horizontal positions. When the focal point is at the centre of the cell, the second run-dependent parameter is at 7.8 cm, so the first cut will be to select this particular position, shown in figure 5.2.

The data we require are in channel 2, so a cut to choose channel 2 must be included, and the effect of this cut is shown in figure 5.3. It can be seen that the number of events roughly halves, and the block of data at $(t - t_{01}) = 0$ vanishes.

To ensure that no cosmic ray muons trigger an event, a start-time greater than zero must be used as a constraint, and this is illustrated in figure 5.4. Obviously in this sample, a cosmic muon did not trigger a single event.

The next constraint that is needed is to make sure that only one pulse on the wire is plotted, and as the main pulse is the first pulse, setting IHIT=1 will ensure this is the case, and this is illustrated in figure 5.5. This also ensures that pulses formed from the overshoot of the amplifier are not considered. Many more pulses are now eliminated from the data sample.

A height cut of less than 1000 (figure 5.6) is useful, as this cuts out all data which has overflowed the amplifier. (Figure 4.12 demonstrated this effect, where the point at 750 V is chopped.) Small pulses can be eliminated by putting in a charge or height cut. A height cut of greater than 50 (figure 5.7) to greater than 100 (figure 5.8) is used to eliminate small noise pulses.

As previously mentioned, the run used to illustrate the cuts selection is a data sample built-up from many individual data samples. It is expected that more ionization will occur when the focal region is moved away from the centre of the cell. As the beam and its profiles are Gaussian, it is reasonable to expect that the drift time profile should be Gaussian too. Figure 5.9 shows the distribution of drift-times

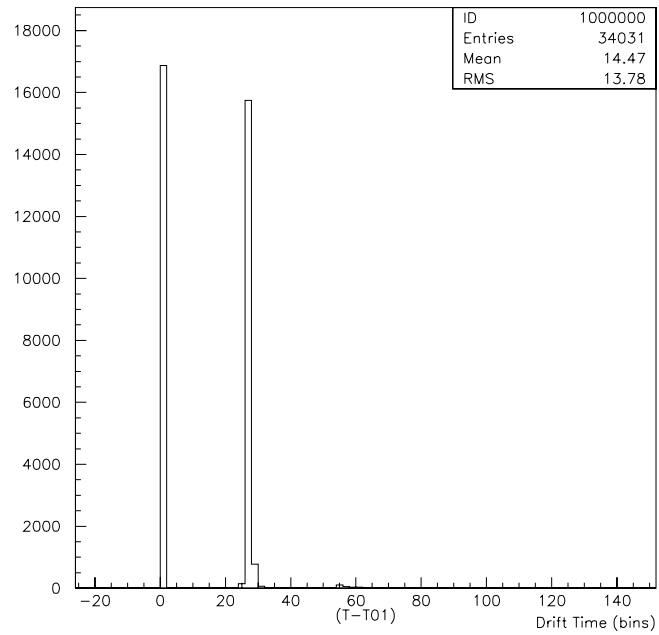


Figure 5.1: The Drift-Time Distribution When No Cuts Are Applied

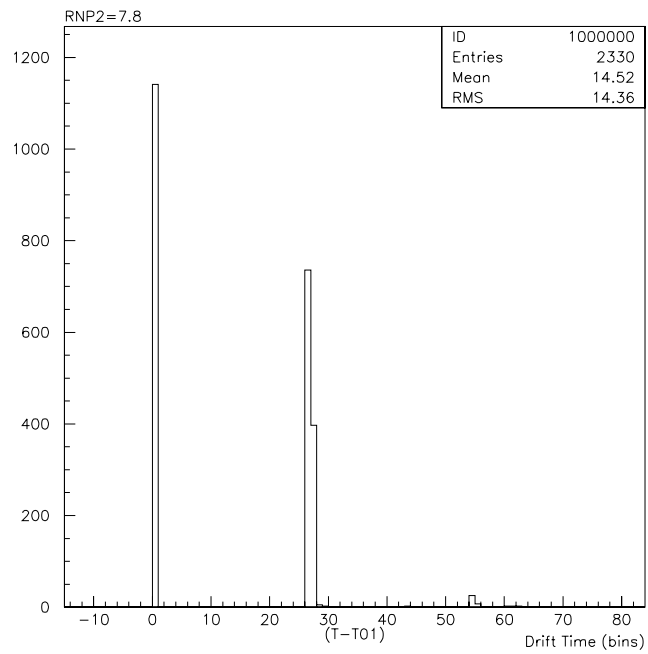


Figure 5.2: The Drift-Time Distribution At The Focal Point

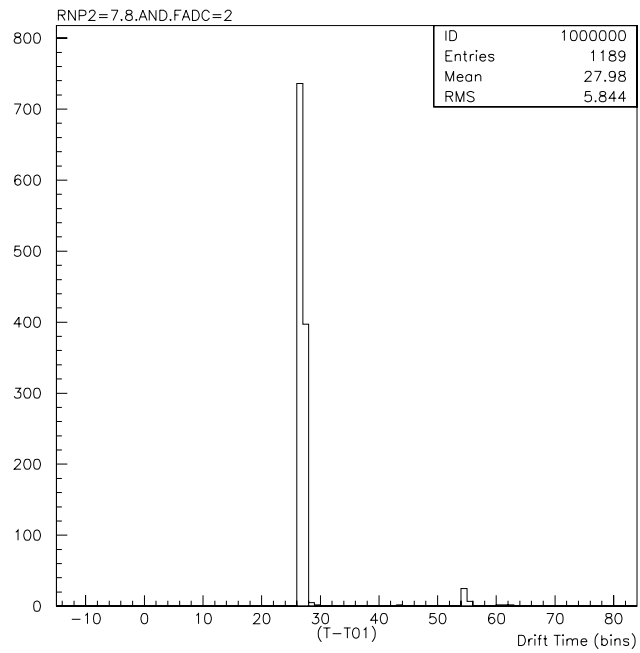


Figure 5.3: Specifying The Correct Channel From The Flash ADC

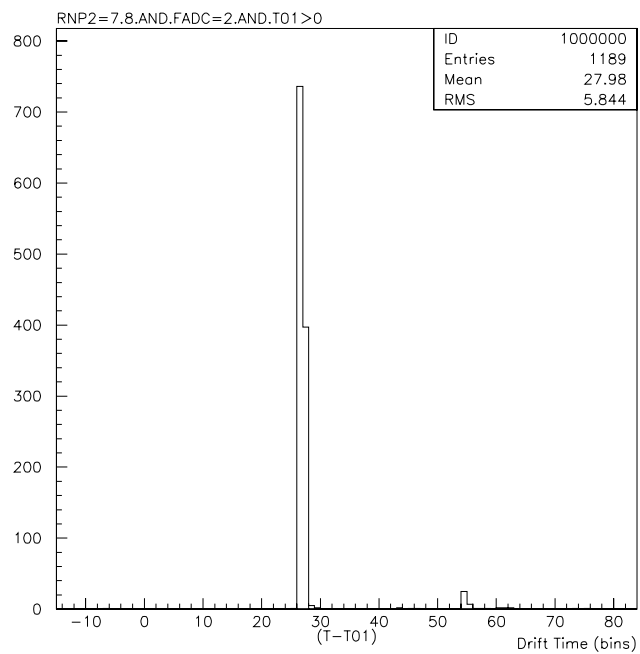


Figure 5.4: Adding A Cut To Stop Cosmic Triggers

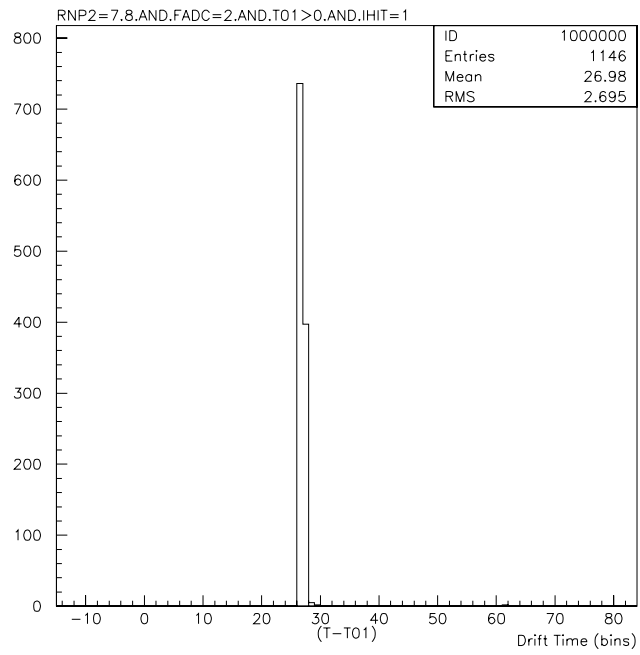


Figure 5.5: Drift-Time Distribution For The First Hit On The Wire.

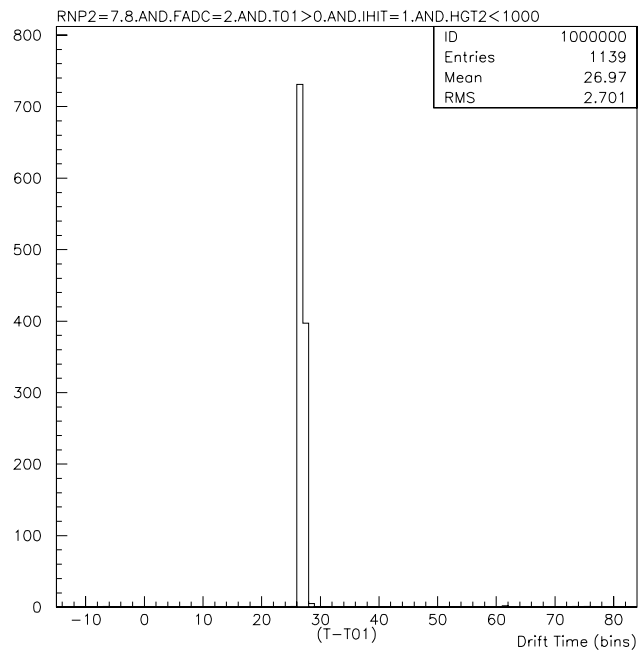


Figure 5.6: Cutting Down Pulses Which Are Too High

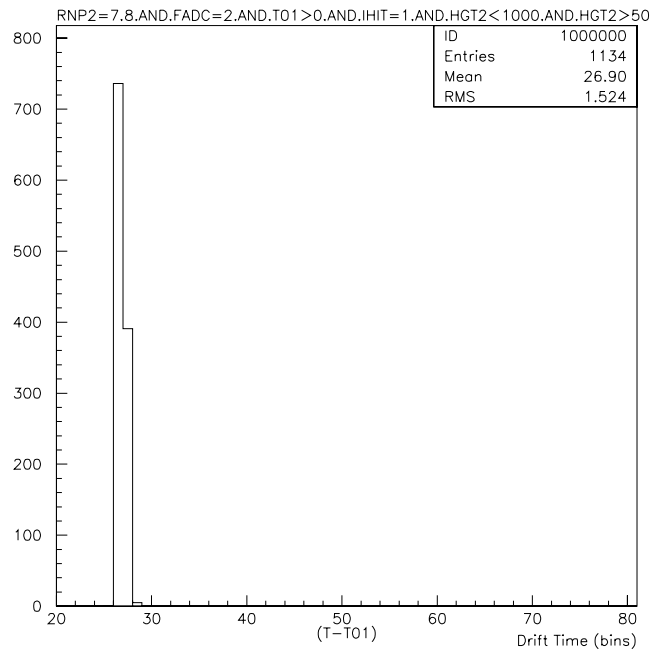


Figure 5.7: Eliminating Small Pulses

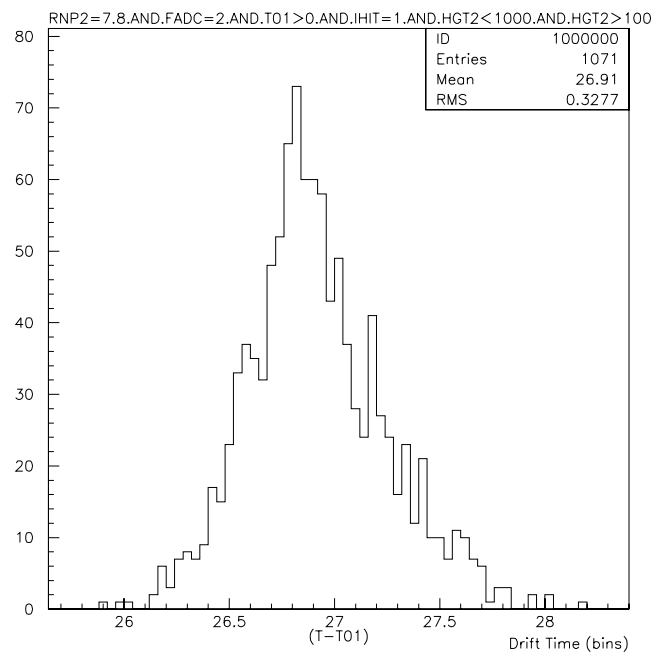


Figure 5.8: Eliminating Slightly Larger Pulses

for the case described above, and figure 5.10 shows a Gaussian envelope fitted to the profile (see section 5.5 for details on how to fit in PAW). It can be seen from the statistical data that the fit is very good.

The user-defined parameters RNP1,2,3 have previously been defined as vertical height of chamber, focal position, and atmospheric pressure respectively. Therefore, to obtain a drift-velocity plot across the cell, one needs to plot what is known as a scatter plot which plots the drift-time against vertical position, illustrated in 5.11.

Once a set of cuts has been decided upon, they can be input into a logical unit, \$3 for example (or any number), to avoid tedious typing for every plot.

It is possible to add many ntuples together into what is called a “chain” in PAW. This was done with many scans through the focal point, at several vertical positions, so that drift-velocity information could be extracted from the separately-gathered information. The same kind of cuts can now be used, with some minor modifications, when dealing with the chain.

Since the individual ntuples are effectively histograms of $(t - t_{01})$ against focal position (RNP2) at a specific vertical position (RNP1), to obtain the drift-velocity curve at the focal point, a particular RNP2 must be specified to work at. As the centre of the cell has been measured, and calculated to correspond to 7.8 cm on the “scale” then one needs to include this constraint in the cuts also.

5.3 Box Plots

It is sometimes instructive to plot a scatter plot as a box plot. This means that PAW draws boxes proportional in size to the density of points at that region. This can be seen in figures 5.11 and 5.12 - one a straight-forward scatter plot, the other a box plot of the same data. Although useful in determining regions of greatest density and for following trends more easily, it is not used in the numeric-extraction analysis.

Graphs such as figures 5.11 and 5.12 show the overall structure of the

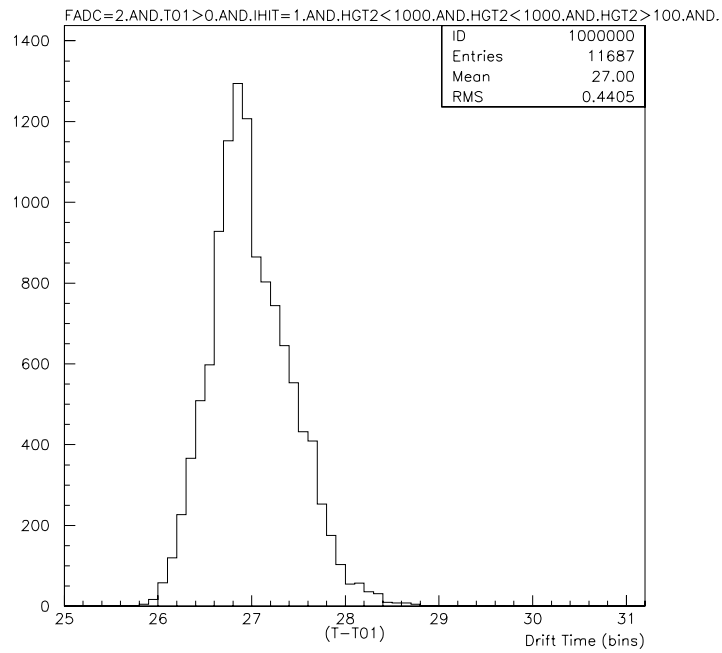


Figure 5.9: Drift-Time Distribution For Run 2916

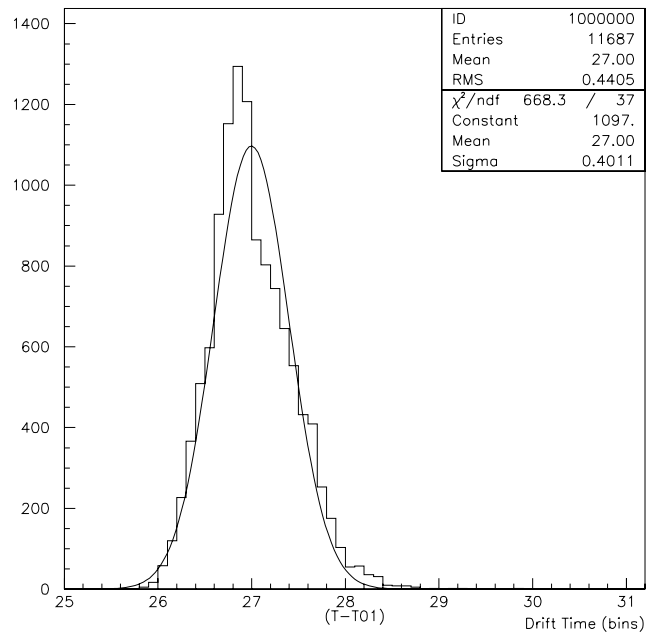


Figure 5.10: Drift-Time Distribution For Run 2916 With A Gaussian Envelope

curves, but they plot all the data points, individually.

What is required is some method of putting these graphs into a histogram, with a mean value calculated from the data at each point, and an error associated with every point.

There is a facility for doing this on PAW. It can be done by creating what is known as a profile histogram, and filling it with the appropriate data.

5.4 Profile Histograms

Profile histograms accumulate statistical quantities of a variable, y , (Drift-time ($t - t_{01}$) in our case) in bins of a variable, x (Drift-distance). The error on the drift-distance is the bin width, being grossly exaggerated. The actual error is far too small to be seen on the graph. One must first create the empty histogram with the correct number of bins and the scale properly defined. The profile histogram can then be filled by a scatter plot. This gives a plot with a point at the middle of the bin, with a horizontal line through it showing the extent of that bin. The vertical lines through every point are the r.m.s. error bars on those points, calculated from the data sample.

If the scale is too large, then one can zoom in on the graph by adjusting the maximum and minimum values of the graph. This cuts out any unwanted blank space above or below the highest and lowest points respectively so that the shape of the graph may be more clearly seen. Also, selected bins can be plotted, by stipulating over which range of bins the histogram should be plotted.

5.5 Fitting in PAW

The last feature that is needed so that a full analysis can be performed is the fitting tool in PAW. A histogram may be fitted with a variety of PAW fits, or an user-defined function for something more complicated than a polynomial or

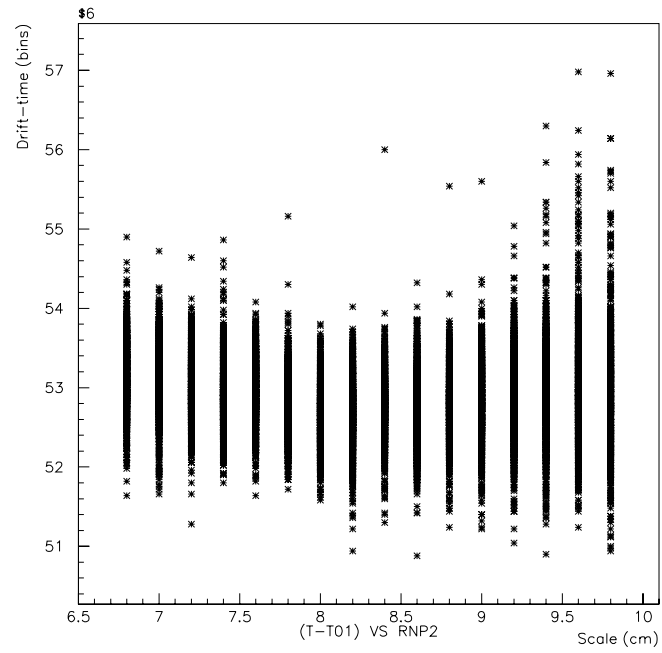


Figure 5.11: Scatter Plot Of Drift-Time With Focal Distance

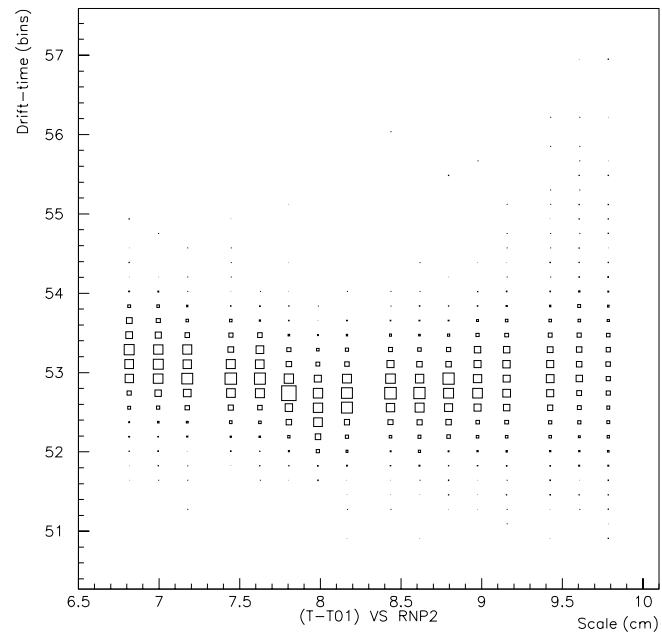


Figure 5.12: Box Plot Derived From The Previous Scatter

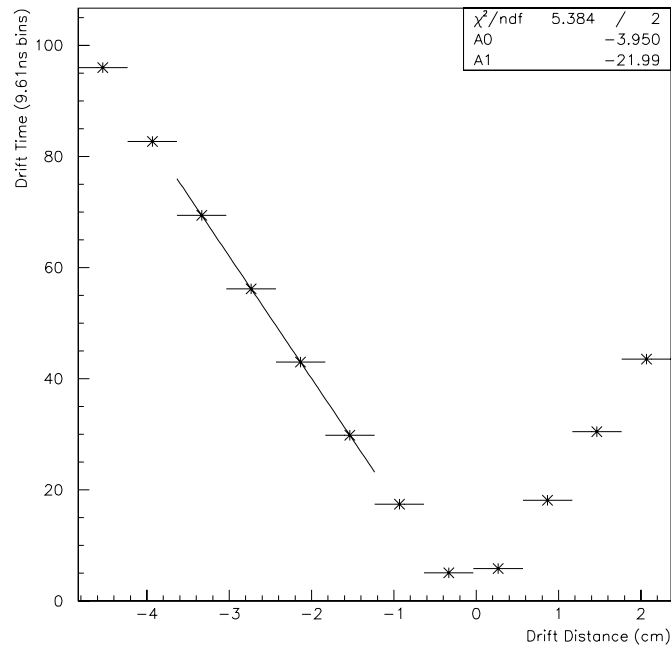


Figure 5.13: Profile Histogram - Central Portion Fitted With Straight Line

Gaussian fit. Fortunately, polynomials (and sometimes Gaussians) were all that were ever required. A Gaussian fit has been illustrated in figure 5.10.

To evaluate the drift velocity, one has to assume that the drift velocity is constant across the middle of the cell, then fit that portion with a straight line, or first-order polynomial. For example, if the central region of the cell lies between bins 3 & 6 (inclusive) in the profile histogram, then only those bins should be fitted with a polynomial of order 1 (a straight line). Figure 5.13 shows just such a fit.

As can be seen from this graph, two coefficients are given to the fit, as well as the χ^2 and the number of degrees of freedom. It is instructive to show a residual plot at this point. A residual plot shows how far from the fitted line the points actually lie. It is obtained by subtraction of the fitted data from the actual data, and the resultant values plotted as a scatter about zero. A residual plot for figure 5.13 is shown in figure 5.14.

A0, the intercept, gives information about the t_{01} determination, and

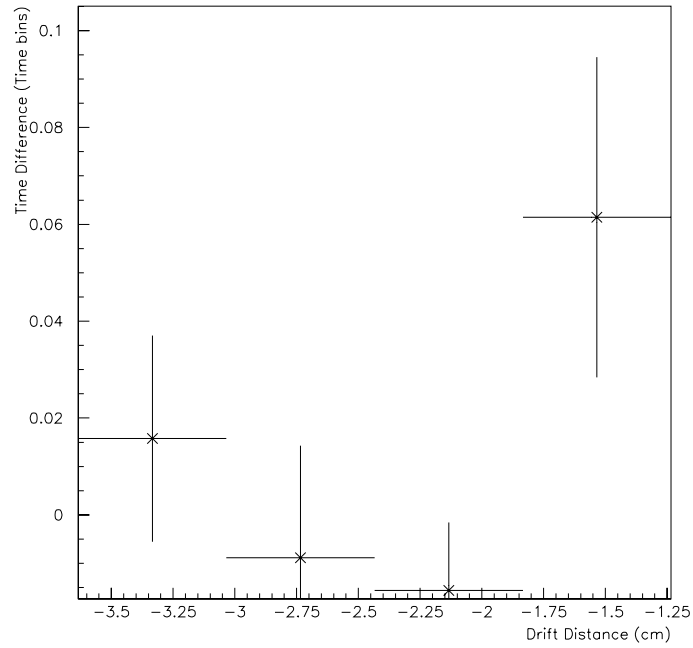


Figure 5.14: Residual Plot Of The Previous Graph

should be very similar in all graphs. $A1$, the slope, gives information about the velocity. $A1$ gives the slope in units of time bins/cm, which is the reciprocal, dimensionally, of a velocity. It can be shown that the relationship between the drift-velocity and the slope is

$$v_{Drift} = \frac{1000}{\text{bin-width}} \times \left| \frac{1}{A1} \right| \text{cm}\mu\text{s}^{-1}$$

As discussed in chapter 4 an investigation of the binning was performed, and the bin width found to be 9.664 ns, experimentally. However, the clock speed (see section 4.5) gave bins 10 ns wide, exactly, therefore,

$$v_{Drift} = \frac{1000}{10} \times \left| \frac{1}{A1} \right| \text{cm}\mu\text{s}^{-1}$$

or

$$v_{Drift} = \left| \frac{100}{A1} \right| cm \mu s^{-1}$$

Now that a formula has been found for calculating the drift velocities, the results can be obtained, and they are presented below.

5.6 Results

Figure 5.15, shows the typical form of the drift-time against drift-distance curve. This particular curve was drawn from data taken at voltages of 2881 V on the electrodes, 4261 V on the sense wire, and at an atmospheric pressure of 1017 mbar. This corresponds to an \mathbf{E} -field of 444.54 V/cm, or $\frac{E}{p} = 437.11$ V/cm.bar. Figure 5.16 shows a profile histogram of the same data. The graphs that are illustrated here show the nature of the space-time relationship across the cell. The central portion is linear, whereas the portion close to the wall and wire deviate from linear behaviour, which is more clearly observable in the profile histogram.

All of the graphs, taken at different voltages, are similar in shape, but with different gradients and intercepts, therefore the relevant information from all the graphs has been collated into table 5.2

From this table, a graph of the drift-velocity against $\frac{E}{p}$ can be drawn and compared to what is expected from simulation. The simulated data are shown first in figures 5.17, 5.18, and 5.19, and the curve obtained from the data taken at Manchester is shown in figure 5.20, with a zoom on the region believed to be the peak shown in figure 5.21.

Taking the graphs at nominal voltages of 2880 ± 1 V, and 4260 ± 1 V, it can be seen that, plotting them against $\frac{E}{p}$, a large variation in drift-velocity is found, which should not be. This implies a degree of irreproducibility in the experiment, as these results were taken in a variety of different ways, i.e., immediately after the volts had been set, a few hours later giving time to settle, and a few days later. Perfect reproducibility is impossible due to the slight changes in atmospheric conditions every time a run is repeated, but if this truly is the plateau region, then

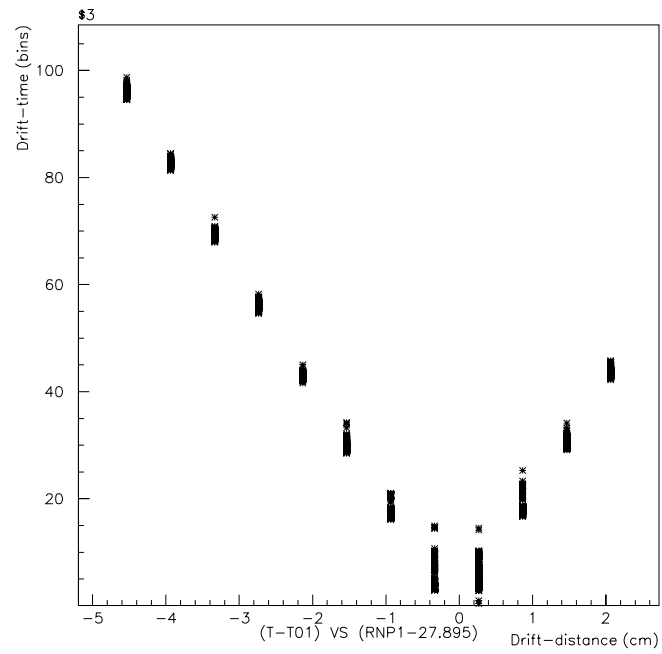


Figure 5.15: Typical Shape Of The Drift-Time Against Drift-Distance Curve

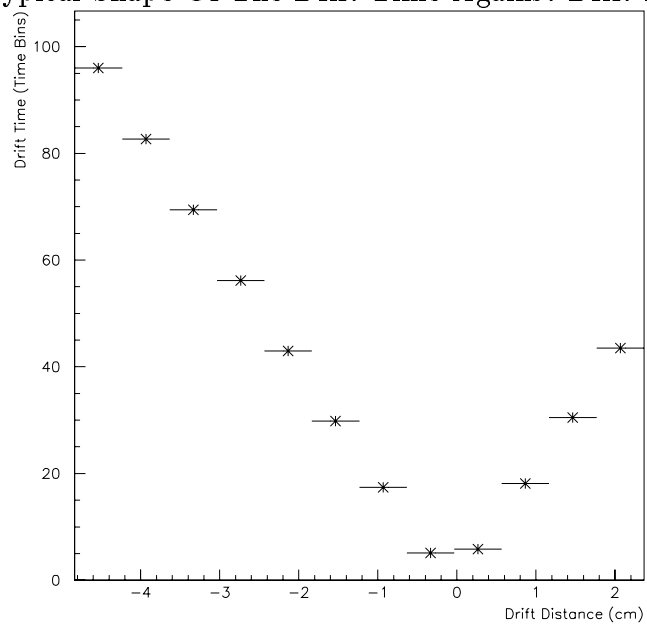


Figure 5.16: Profile Histogram Of The Drift-Time Against Drift-Distance Curve

Sense Voltage V \pm 1V	Drift Voltage V \pm 1V	$\frac{E}{P}$ V/cm.bar	A0 (Intercept) bins	A1 (Slope) bins/cm	Drift Velocity cm/ μ s
3437	2000	304.93 \pm 0.50	-11.122 \pm 0.103	-27.711 \pm 0.045	3.609 \pm 0.006
3714	2300	350.65 \pm 0.49	-5.623 \pm 0.086	-23.894 \pm 0.038	4.185 \pm 0.007
3992	2600	396.39 \pm 0.54	-4.926 \pm 0.078	-22.823 \pm 0.030	4.382 \pm 0.006
4130	2750	418.04 \pm 0.58	-4.425 \pm 0.063	-22.494 \pm 0.024	4.446 \pm 0.005
4149	2770	420.67 \pm 0.53	-4.705 \pm 0.056	-22.527 \pm 0.022	4.439 \pm 0.004
4177	2800	425.22 \pm 0.57	-4.603 \pm 0.061	-22.449 \pm 0.023	4.455 \pm 0.005
4194	2820	428.24 \pm 0.57	-4.414 \pm 0.057	-22.344 \pm 0.022	4.475 \pm 0.004
4223	2850	432.40 \pm 0.56	-4.330 \pm 0.062	-22.262 \pm 0.023	4.492 \pm 0.005
4261	2881	437.11 \pm 0.58	-3.950 \pm 0.045	-22.307 \pm 0.002	4.483 \pm 0.0004
4261	2881	437.54 \pm 0.55	-4.032 \pm 0.060	-22.249 \pm 0.023	4.495 \pm 0.005
4260	2880	438.24 \pm 0.58	-4.284 \pm 0.039	-22.246 \pm 0.015	4.495 \pm 0.003
4260	2880	438.67 \pm 0.54	-4.686 \pm 0.053	-22.464 \pm 0.020	4.452 \pm 0.004
4260	2880	439.08 \pm 0.59	-3.676 \pm 0.055	-21.995 \pm 0.021	4.546 \pm 0.004
4260	2880	439.10 \pm 0.59	-4.211 \pm 0.030	-22.163 \pm 0.013	4.512 \pm 0.003
4261	2881	440.79 \pm 4.46	-5.121 \pm 0.014	-22.483 \pm 0.005	4.448 \pm 0.001
4260	2880	441.26 \pm 0.58	-3.944 \pm 0.100	-22.227 \pm 0.048	4.499 \pm 0.010
4278	2900	444.33 \pm 0.57	-3.701 \pm 0.121	-22.250 \pm 0.051	4.494 \pm 0.010
4300	2930	448.92 \pm 0.61	-4.153 \pm 0.111	-22.343 \pm 0.045	4.476 \pm 0.009
4324	2950	452.00 \pm 0.60	-4.067 \pm 0.081	-22.314 \pm 0.031	4.481 \pm 0.006
4371	3000	459.66 \pm 0.56	-3.903 \pm 0.079	-22.194 \pm 0.033	4.506 \pm 0.007

Table 5.2: Collected Data From Drift Velocity Measurements At Various Values Of

$$\frac{E}{P}$$

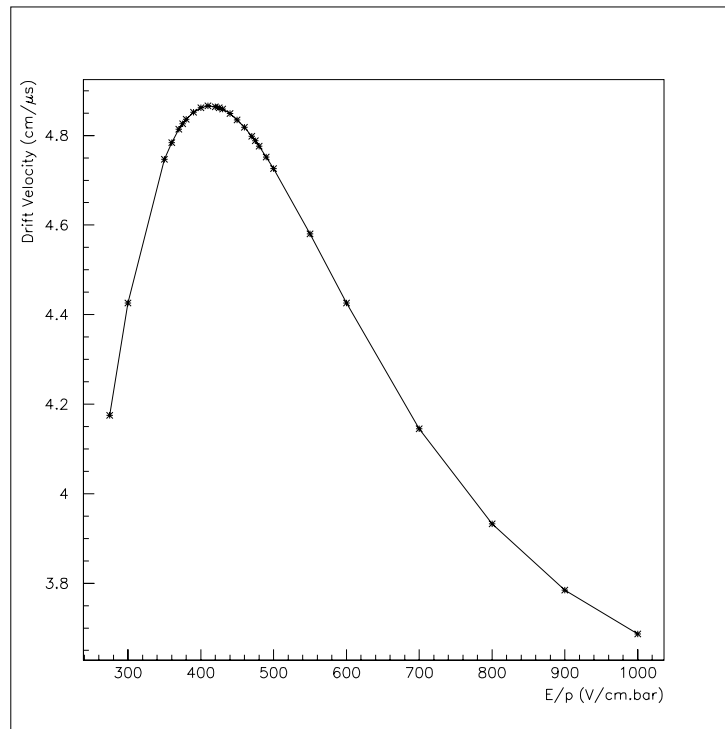


Figure 5.17: Variation Of Drift-Velocity With $\frac{E}{p}$ For The Manchester Gas

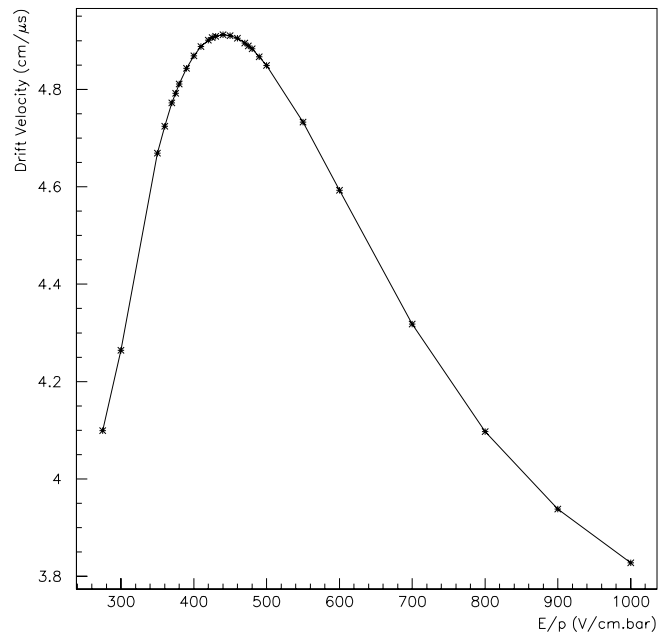


Figure 5.18: Variation Of Drift-Velocity With $\frac{E}{p}$ For The H1 Gas

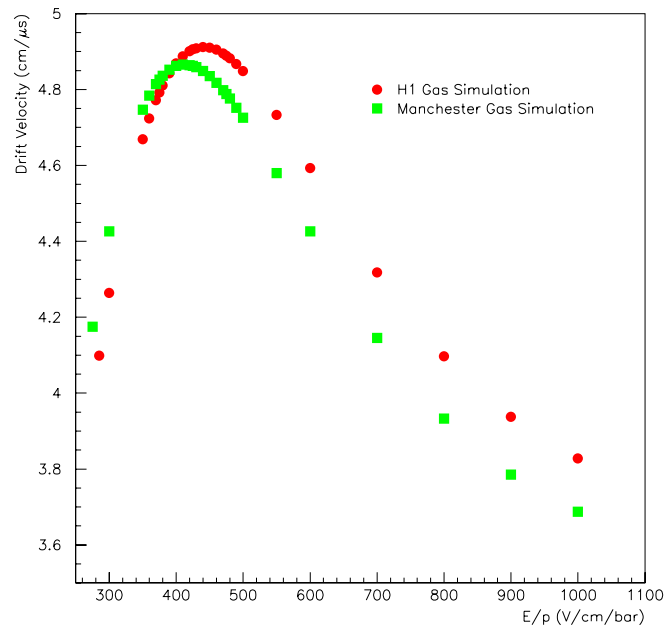


Figure 5.19: Both The Previous Graphs For Easier Comparison

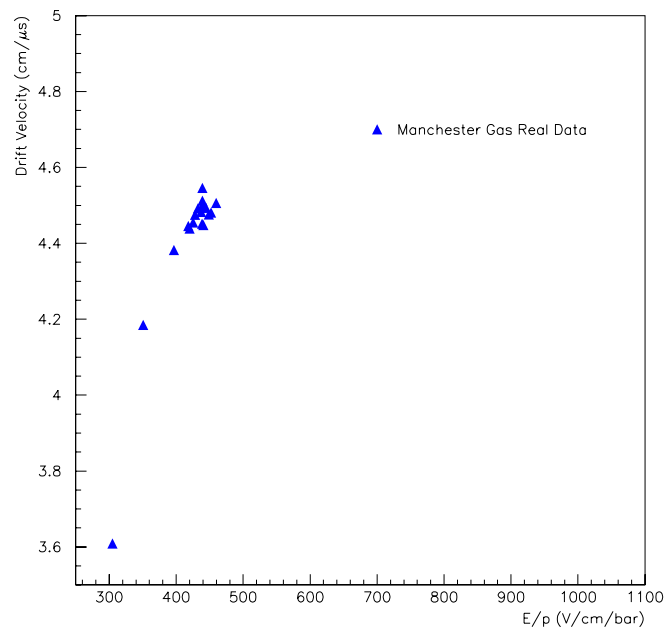


Figure 5.20: Real Drift Velocity Against $\frac{E}{p}$ For The Gas At Manchester

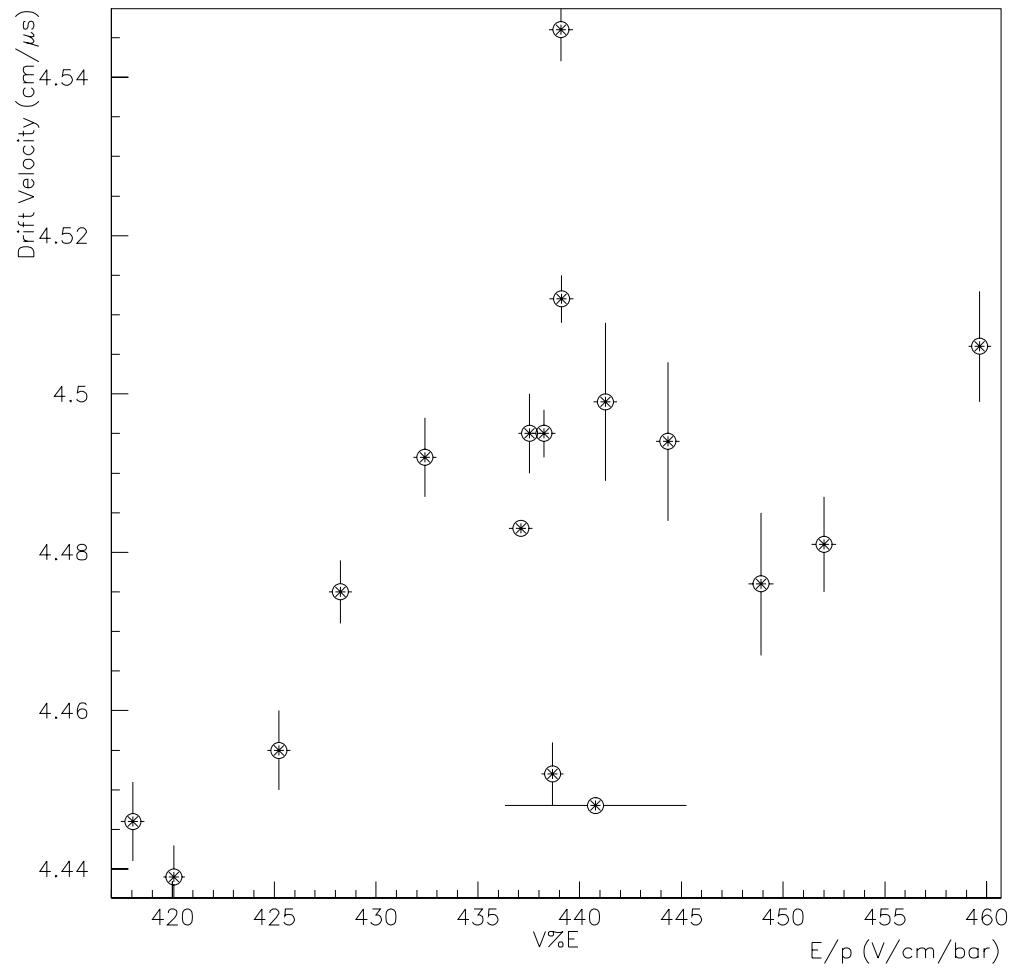


Figure 5.21: Zooming In On The Peak

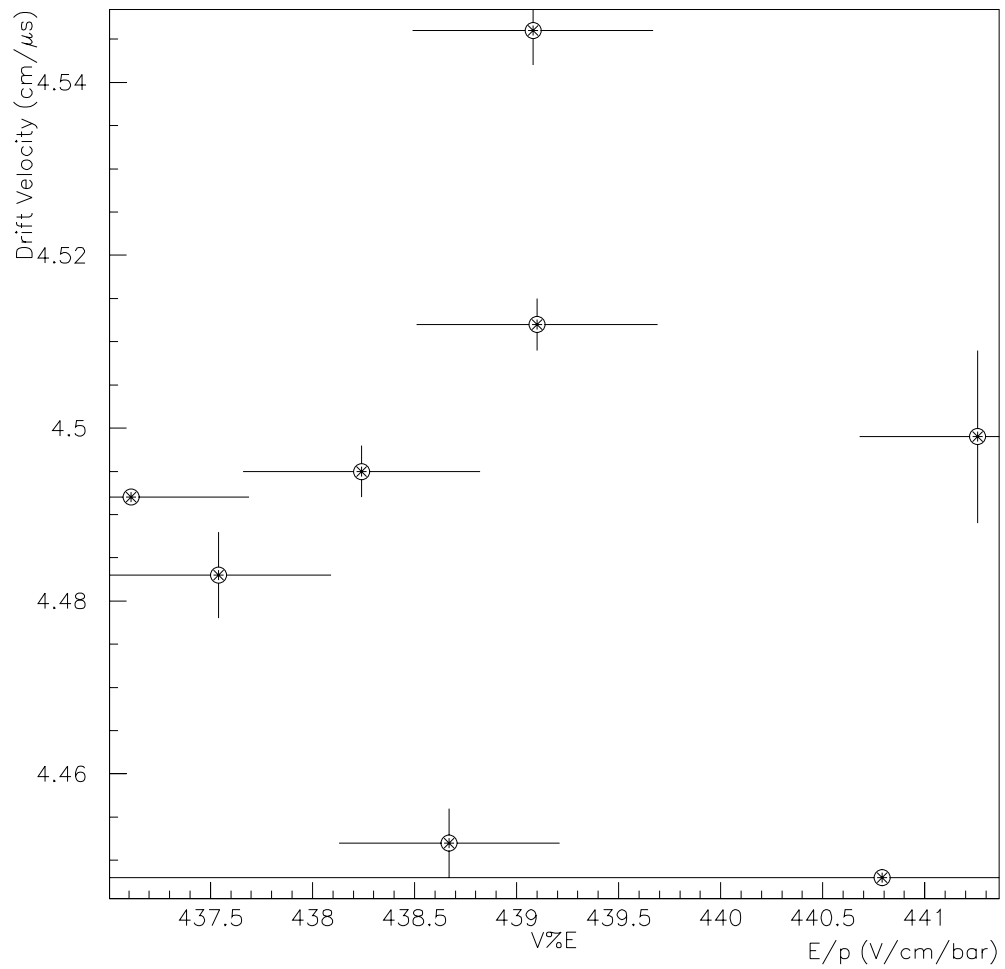


Figure 5.22: Scatter in the Drift-times at the same Operating Voltages but different pressures

the velocities should be more consistent. Figure 5.22 illustrates this problem clearly.

It is now possible to superimpose both the simulated data and the real data on the same graph, and the result is shown in figure 5.23. It can be seen that, although the real data follow the broad shape of the curve, the actual values are considerably lower than expected.

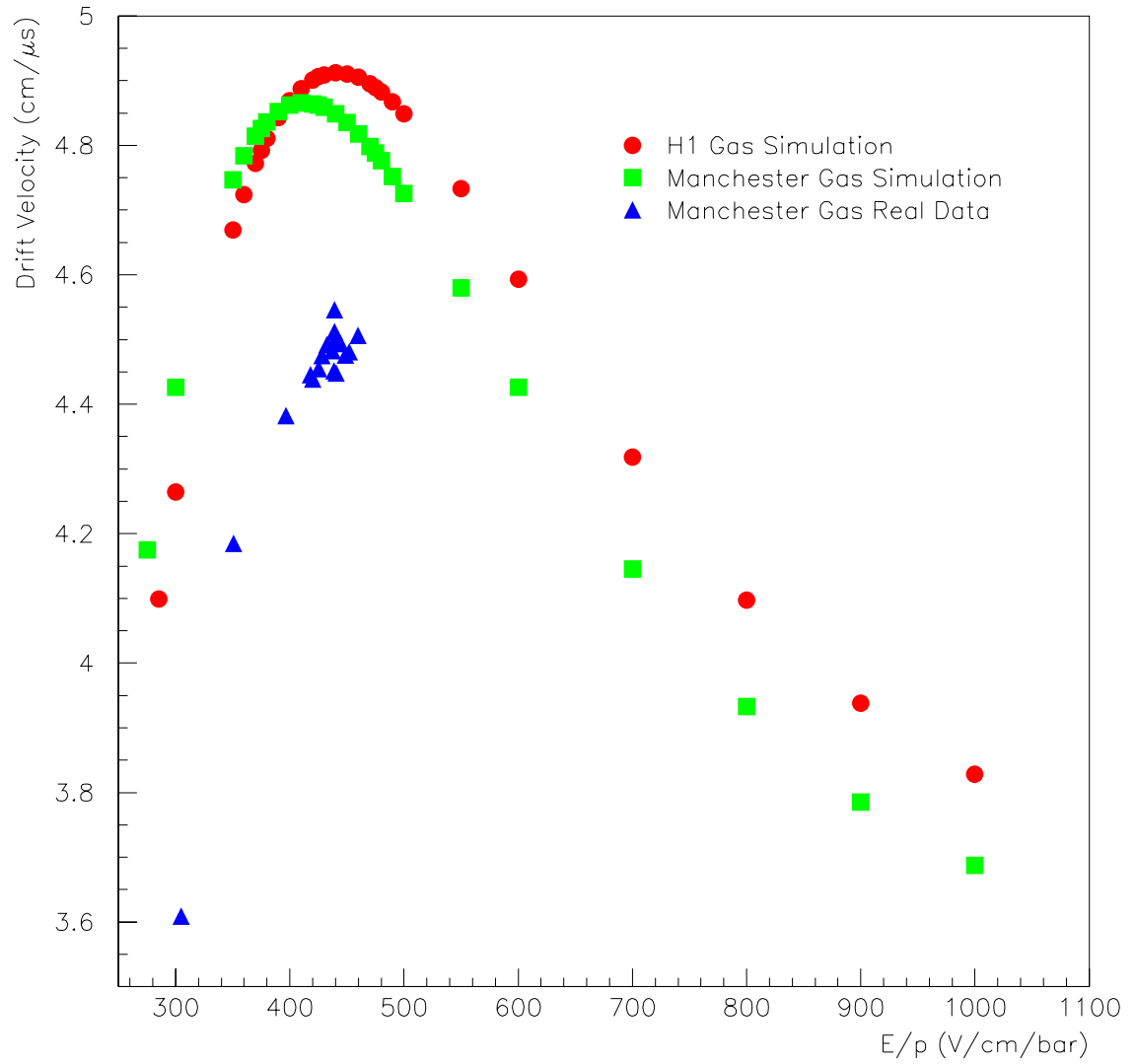


Figure 5.23: Comparison Of Simulation And Real Data

Chapter 6

Discussion

It was found from experiment that the focal-spot size was $\sim 70 \mu\text{m}$ for a 25 mm lens, which is excellent as this is much smaller than the cell resolution ($\sim 200 \mu\text{m}$ at best).

To simulate a muon properly however, we would require a straight beam with no waist or divergence. As has been shown, the lens that was worked with, 100 mm, gives a fairly tight focal region, providing ionization from a small volume in the cell. A muon should really be simulated by at least a 300 mm lens as the length of the waist is larger, but the constraints of the room size prevent any focal lengths greater than 300 mm from being used. Perhaps a better idea would be a series of lenses to reduce the beam to a waist, then at its focus another lens could be placed (in effect a telescope) to produce a parallel beam again, but of a much smaller size than the original - much smaller, in fact, than the cell resolution - providing a better simulation of a muon. Again, constraints of room size would be a factor for consideration. The simplest method would be to remove the lenses altogether, and allow the parallel bundle to pass through the cell unfocussed. However, such an unfocussed beam would be much too broad (diameter $\sim 2 \text{ mm}$) for any precise measurement.

The time binning investigation proved that, although the FADC, governed by the clock on the Scanner, operates at 100 MHz giving 10 ns time bins, when

investigated, the width of the bin was found to be 9.664 ns. This is $\sim 4\%$ effect, which is significant when dealing with such precisely measured quantities. This discrepancy is puzzling, and no explanation can be offered apart from a delay being introduced into one measuring method which is not there in the other.

Investigation of the shape of the v_{Drift} against $\frac{E}{P}$ curve shows behaviour reasonably consistent with the simulation, but higher fields couldn't be investigated for fear that the wire may break, or breakdown occurring inside the chamber. Even though the curve is roughly of the right shape, the actual slope and maximum point are not similar to the predicted value. The values obtained here are lower than those expected from simulation. This could be due either to the gas not being exactly what BOC claims it to be, or an error in the simulation, a flaw in the chamber replica, or some other unexplained variable. Without further evidence to prove or disprove the possible causes, or high-field measurements to see where the plateau region really lies, it is impossible to tell what is at fault.

From figure 5.22 it can be seen that there is a large spread in the drift-velocities with only a small change in $\frac{E}{P}$. This would seem to indicate that we are not working at the plateau, but on a slope either just before or just after the plateau, and that changes in pressure change the drift-velocity markedly. Another, though unwelcome, explanation is that there is a certain degree of irreproducibility in the experiment, but its cause is unknown.

The average value for the drift-velocity at the nominal operating voltages, taking no account of the pressure variation, is $4.491 \pm 0.035 \text{ cm}\mu\text{s}^{-1}$. If each v_{Drift} is normalized by dividing by $\frac{E}{P}$ for each one, and then averaging these, multiplying the result by the average field, a value of $4.491 \pm 0.064 \text{ cm}\mu\text{s}^{-1}$ is obtained. The value is exactly the same, with roughly double the error, again seemingly corroborating the linearity of the region in which the data were taken - indicating that the region is indeed the plateau.

This irreproducibility in the results is worrying, though possible causes for the inconsistency are pressure variations measured in the laboratory may not be exactly the same as those inside the cell, or that the cell is slower to respond to these pressure changes than the digital barometer is. Another possible cause is that the pressure differences are affecting the flow-rate of the gas, in that a higher

pressure at the exhaust will inhibit flow more than a lower pressure would, and this difference in flow rate would affect the drift-velocity.

The graphs were also checked for some other systematic error, by plotting the data points in the order in which they were taken, but no pattern of any kind was found, thus eliminating the possibility of a hidden systematic error.

It is possible that the voltages recorded on the monitor for the supply are not what are on the electrodes or the wire itself, which means that we are recording a voltage which is too high compared to the actual voltage. Figure 5.23 seems to indicate that this is so, as the data points would “fit” the simulated curve better if they were at a lower \mathbf{E} -field. If only one of the voltages is incorrect, and the difference between sense and drift voltages is lower than anticipated, then this would affect the gas gain. Typically a value of $\sim 10,000$ is expected, but if the voltages are lower, then the gain will become drastically lower, and if the difference is small enough, then the gain would be 1, i.e., no signal at all. It is reasonable to believe, from the raw data, that the gas gain is approximately correct, and, consequently, that the voltages are too.

Previous results for the same drift cell[17] gave a drift-velocity of $\sim 4.55 \text{ cm}\mu\text{s}^{-1}$.

It was thought that, because the value used at H1 is the *average* drift-velocity across the whole cell, then the drift-velocity obtained at Manchester by just fitting the central portion would be too low. The whole curve was fitted, and differences in both the slope and the intercept were found (leading to second decimal place variations in the drift-velocity) however, they are far too small to account for the large discrepancy between the values of the drift-velocity at Manchester and H1. Only results from one side of the cell have been presented here (Drift Distance < 0 cm) as a full range of values on both sides of the wire is not possible, though the few data points obtained (Drift Distance > 0 cm) have been fitted giving the same results, but because of considerably less statistics, the fit is obviously far poorer.

Chapter 7

Conclusion

Although lots of work has been done this year, there is no acceptable value that can be given to the drift velocity. A value of $4.491 \pm 0.035 \text{ cm}/\mu\text{s}$ may be quoted as the value found for the cell and gas composition at Manchester. This is inconsistent with the value used at H1 in their drift chambers and for their gas. It is not unexpected that the drift velocities are not identical, though such a large difference is somewhat surprising.

The conclusions that may be drawn from all the previous chapters are:-

Either the drift cell is not as good a replica of those at H1 as originally thought; or the simulation finds a value for the drift velocity which is too high; or there is some fault in the electronics causing a binning problem; or the lens may not be focussed *exactly* on the centre of the cell, though this would be a small effect; or the voltages on the chamber are not what they are believed to be.

Possible work for next year could be:-

A more thorough investigation of the binning, to see exactly where the discrepancy lies;

Direct measurements of the voltage from the chamber itself, and not from the monitor. This should be possible by removing a panel on the rear side of the

chamber and measuring it from there. This would confirm whether the correct voltages are being used or not;

“Rapid-fire” measurements of the drift-times at fixed locations in the cell, then going back for repetition immediately, i.e., data at, say, 4 vertical positions, then an immediate repeat to see if they are consistent;

Finding a more accurate method of focussing the beam.

It would also be beneficial if gas more closely resembling that used at H1 could be used.

Bibliography

- [1] Jönsson, L., *et al.*, *Nuclear Instruments and Methods in Physics Research A* **340** (1994) 304-308
- [2] Mehta, A., *Diploma: Investigation of the Drift Velocity of the Forward Muon Drift Chambers of the H1 Detector*, (May 1991) 31.
- [3] Sauli, F., *Principles of Operation of Multiwire Proportional and Drift Chambers*, Lectures given in the Academic Training Programme of CERN (1975-76) 74-75.
- [4] Mehta, A., *Diploma: Investigation of the Drift Velocity of the Forward Muon Drift Chambers of the H1 Detector*, (May 1991) 38.
- [5] Biddulph, P., *Private Communication*.
- [6] Bispham, P., *Diploma: Laser Calibration of the Forward Muon Drift Chambers of the H1 Detector* (June 1993) 24
- [7] British Oxygen Company, *Gas Composition Report*.
- [8] Biagi, S., *MAGBOLTZ Simulation*, *Nuclear Instruments and Methods in Physics Research A* **283** (1989) 716.
- [9] Milonni, P.W. and Eberly, J.H., *Lasers*, John Wiley & Sons, 1988 p.415.
- [10] Foster, J., *Private Communication*.
- [11] Milonni, P.W. and Eberly, J.H., *Lasers*, John Wiley & Sons, 1988 p.487.
- [12] Hecht, E., *Optics 2nd Edition*, Addison Wesley, 138.

- [13] *Handbook of Chemistry and Physics*, CRC Press Inc., 61st edition (1980-81), E-392.
- [14] Jenkins, F.A., and White, H.E., *Fundamentals of Optics 4th Edition*, McGraw Hill, 552.
- [15] Bispham, P., *Diploma: Laser Calibration of the Forward Muon Drift Chambers of the H1 Detector* (June 1993) 21,40.
- [16] Bispham, P., *Diploma: Laser Calibration of the Forward Muon Drift Chambers of the H1 Detector* (June 1993) 24-27.
- [17] Bispham, P., *Diploma: Laser Calibration of the Forward Muon Drift Chambers of the H1 Detector* (June 1993) 44.

Acknowledgements

I would like to thank Dr. Mike Ibbotson, my supervisor, for his constant help and assistance throughout the year and Dr. Joe Foster for the software support side of things, and especially for the PAW tutorials! Enormous amount of thanks also to Ray Thompson and Julian Freestone, without who's constant supply of good humour, and unnerving knowledge of the experiment and electronics, this thesis would be considerably shorter! Thanks must also go to Dr. John Banks for his instant replies to questions starting with "John, how do you do... in Unix or VMS" and other abstruse computing questions!! Thanks must also go to the rest of the group for such thorough instruction in the arcane ways of HEP!

I would also like to thank "The Butty Club" especially Fred and Dave for the weird, wacky and wonderful lunchtime conversation, ranging from the sublime to the ridiculous - cavity wall insulation (a regular favourite) to exploding seagulls!!, and Roger for the crossword help when we, invariably, became stuck!

And now for the roll of honour... Thanks to:

The other 7 students in my year, Andrew, Ben, Jane, Jim, Nick, Ollie, and Sue, for providing a good environment to work(!) in

The rest of the HEP (and honorary HEP!) clan Allan, NickT, Perry, PeterC, Rob, and Stuart for their good humour and (occasional!) help. Good luck with FREEDRUGALIEN, Stuart. Whoever's reading this - GO AND SEE THEM!!!! BUY A TAPE FROM stuart@h1.ph.man.ac.uk

My housemates (who requested a credit!) Emily and Moyeen, for being such fun people to share a house with, and for utterly banal and childish behaviour!

The "Glengower Swift Pint Before Closing Time?" Club, that dynamic duo, Damian and Jason, and for the High Table Dinners - long may it continue... remember guys "we're not like other people - we're *Artists*"

And last, but definitely **NOT** least, my parents, without whose help and support, none of this would have been possible. *Diolch o waelod calon*